Evaluation of aerosol- and gas-phase tracers for identification of transported biomass burning emissions in an industrially influenced location in Texas, USA

Sujan Shrestha[1], Shan Zhou[2,3], Manisha Mehra[1], Meghan C. Guagenti[1], Subin Yoon[2], Sergio L. Alvarez[2], Fangzhou Guo[2,3], Chun-Ying Chao[3], James H. Flynn III[2], Yuxuan Wang[2], Robert J. Griffin[3,4], Sascha Usenko[1], Rebecca J. Sheesley[1*]

[1]Department of Environmental Science, Baylor University, Waco, TX, USA

[2]Department of Earth and Atmospheric Sciences, University of Houston, Houston, TX, USA

[3]Depertment of Civil and Environmental Engineering, Rice University, TX, USA

[4]School of Engineering, Computing, and Construction Management, Roger Williams University, Bristol, RI, USA

Correspondence to: Rebecca J. Sheesley (Rebecca_Sheesley@baylor.edu)

Abstract

As criteria pollutants from anthropogenic emissions have declined in the US in the last two decades, biomass burning (BB) emissions are becoming more important for urban air quality. Tracking the transported BB emissions and their impacts is challenging, especially in areas that are also burdened by anthropogenic sources like the Texas Gulf coast. During the Corpus Christi and San Antonio (CCSA) field campaign in Spring 2021, two long-range transport BB events (BB1 and BB2) were identified. The observed patterns of absorption Ångström Exponent (AAE), high-resolution time-of-flight aerosol mass spectrometer (HR-ToF-AMS) BB tracer (f_{60}), equivalent black carbon (eBC), acetonitrile and carbon monoxide (CO) during BB1 and BB2 indicated differences in the mixing of transported BB plumes with local anthropogenic sources. The combined information from HYSPLIT backward trajectory (BTs) and satellite observations revealed that BB1 had mixed influence of transported smoke plumes from fires in Central Mexico, the Yucatan peninsula, and the Central US, whereas BB2 was influenced majorly by fires in the Central US. The estimated transport time of smoke from the Mexican fires and the Central US fires to our study site were not too different (48-54 hours and 24-36 hours, respectively) and both events appeared to have undergone similar levels of atmospheric processing, as evident in the elemental ratios of bulk organic aerosol (OA). We observed a progression of f_{44} vs. f_{60} as a function of time elapsed during BB2. Positive matrix factorization (PMF) analysis of OA showed that BB1 had a mixture of organics from aged BB emission with an anthropogenic marine signal while the oxidized organic compounds from aged BB emissions dominated the aerosols during BB2. While aerosol measurements exhibited good agreement with respect to the BB designation, the CO and acetonitrile trends revealed more complicated source contributions. Our analysis from mobile and stationary measurements highlights that both CO and acetonitrile are likely impacted by local sources even during the BB events and specifically that acetonitrile cannot be used as a unique BB tracer for dilute BB plumes in an industrially influenced location. Finally, we provide evidence of the potential

regional impacts of these transported BB events on urban O_3 levels using measurements from the surface air quality monitoring network in Texas.

1. Introduction

Biomass burning (BB) activities emit fine particulate matter (PM$_{2.5}$, aerodynamic diameter smaller than 2.5 μm), volatile organic compounds (VOCs) and trace gases into the atmosphere. BB plumes can be transported across long distances and impact air quality in downwind locations (Rogers et al., 2020; Sciare et al., 2008; Sakamoto et al., 2015; Streets et al., 2003; Zhang et al., 2012; Morris et al., 2006; Markowicz et al., 2016; Forster et al., 2001). During long-range transport, the physical properties and chemical composition of the plume can be altered significantly by both plume ageing and dilution due to boundary layer mixing (Reid et al., 2005; Hung et al., 2020).

In urban locations that are burdened by local anthropogenic sources, it is challenging to characterize and quantify the impacts of aged and/or dilute BB smoke plumes (Bein et al., 2008; Singh et al., 2012). Several approaches have been established to determine the impact of transported BB smoke on ambient air quality of downwind locations. This includes laboratory, field-based and satellite observations of aerosol composition and optical properties (de Gouw and Jimenez, 2009; Laing et al., 2016; Li et al., 2020; Zauscher et al., 2013; Zhou et al., 2017), and anlayzing chemical and organic molecular markers of BB emissions (including but not limited to carbon monoxide (CO), non-sea salt potassium, black carbon (BC), brown carbon (BrC), acetonitrile and levoglucosan) (Yokelson et al., 2009; Bhattarai et al., 2019; Huangfu et al., 2021; Bond and Bergstrom, 2006; Mehra et al., 2019). Studies based on aerosol optical properties utilize wavelength dependence of aerosol absorption and scattering to identify aerosol type i.e., differentiate between BC from fossil fuel combustion, BrC from BB and minerals from dust (Schmeisser et al., 2017). Absorption Ångström exponent (AAE), scattering Ångström exponent (SAE) and single scattering albedo (SSA) are commonly used intensive parameters to characterize the aerosol wavelength dependence (Bergstrom et al., 2007; Russell et al., 2010; Gyawali et al., 2009; Kirchstetter et al., 2004). In order for molecular or chemical markers to be used in identifying BB contribution, these markers must be conserved during atmospheric chemical reaction during the transport (Fraser and Lakshmanan, 2000). Further, for these markers to be detectable in urban locations, the specific tracer must be unique to BB emission and emitted in large quantity so that the compound is quantifiable above the urban background concentration.

The frequency, duration and burned area during wildfires in the Northwestern US increased over the last two decades under the changing climatic conditions (Westerling and Bryant, 2008; Westerling et al., 2006; Kasischke and Turetsky, 2006), implying an increase in the concentration of air pollutants as a result of these fires. These impacts can be observed on a regional scale (Jaffe et al., 2008). For example, several studies showed that the transported pollutants from BB emissions in the Alaska, Canada and US Pacific Northwest exacerbated ozone (O$_3$), CO, BC and PM$_{2.5}$ levels in Houston, Texas (Lei et al., 2018; McMillan et al., 2010; Morris et al., 2006; Schade et al., 2011). Wildfires and agricultural burning in the Central Mexico and the Yucatan peninsula peaks during spring-summer season and also transports pollutants to the Southern US (Wang et al., 2018; Rogers and Bowman, 2001; Yokelson et al., 2013). It has not been reported whether fires in this region are also increasing. Wang et al. (2018) have shown that the transport of Central Mexican and Yucatan BB emissions adversely impacted surface air quality at several major urban centers along the Gulf Coast, including Houston and Corpus Christi in Texas. The episodic transport events of BB emissions

70   can result in O₃ and PM₂.₅ exceedances of the air quality standards across several metropolitan areas in Texas. The Texas Commission on Environment Quality (TCEQ) operates a network of surface air quality monitoring stations in Texas, but the measurements are largely limited to criteria pollutants. Realtime observational data integrated with satellite observations and transport models may improve efforts to track the transported BB emissions, locate the source regions, understand the plume aging and analyze its impacts on surface air quality.

75   Although Texas is the second-most populous state in the US, with multiple industrial and economic urban centers, many of the previous air quality studies focused on the Houston-Galveston-Brazoria and Dallas-Fort Worth areas (Parrish et al., 2009; McMillan et al., 2010; Yoon et al., 2021; Anderson et al., 2019; Shrestha et al., 2022; Guo et al., 2021). To better understand air quality drivers in emerging Texas cities, the San Antonio Field Study (SAFS) 2017 investigated ambient concentration and sources of VOCs and trace gases as well as physical and chemical processes

80   that control O₃ (Guo et al., 2021; Shrestha et al., 2022; Anderson et al., 2019). Results from the SAFS 2017 study highlighted the need to characterize the influence of upwind sources and long-range transport on air quality in San Antonio. To address these outstanding questions from SAFS 2017, the Corpus Christi and San Antonio (CCSA) Field Study was conducted in spring 2021 (Zhou et al., 2023). Corpus Christi is upwind of San Antonio when the wind is coming from the south-southeast. This mobile and stationary field experiment was designed to measure the impact of

85   local emissions and transported pollution on air quality in Corpus Christi and San Antonio. This manuscript primarily focuses on BB transport events identified during stationary measurement at Port Aransas (PA), a Gulf Coast city near Corpus Christi, during the field campaign (see Fig. 1). The goals were to (i) study the physical and chemical properties of transported BB smoke and their impact on background air quality in PA, (ii) identify fire source regions and understand transport times, aging and dilution of smoke plumes and (iii) evaluate challenges of using BB tracers in an

90   anthropogenically influenced area like PA. Finally, general comments on extending permanent in-situ monitoring networks with low-cost aerosol optical measurements for identifying BB events are offered.

2.   Method:

2.1. Site description

The stationary measurements were performed at a beachfront site in PA, TX (27.803°N, 97.077°W). The sampling

95   site is approximately 4 km southwest of the mouth of the Corpus Christi Ship Channel into the Gulf of Mexico and 35 km directly east of Corpus Christi's urban core. Oil and gas wells lie in every direction from the study site (green star) (Fig. 1a). The instrumentation was housed in a Baylor University/ University of Houston/ Rice University-operated mobile air quality lab (MAQL2). MAQL2 is a 35-m³ insulated air-conditioned trailer with a ~9-m telescoping tower and inlet box that extend above the trailer during stationary measurements (Fig. S1). The aerosol inlet has a

100   PM₂.₅ cyclone and stainless-steel bellows. The inlet lines inside the trailer were made as short as possible (0.5 m); these lengths of tubing were insulated to minimize wall loss and vaporization effects associated with temperature changes between the ambient air and inside the trailer. A heated sampling line set at 70 ℃, manufactured by Atmos-Seal Engineering Inc., was used for VOC measurements. During mobile measurements, the MAQL2 was towed by a Ford F-250 truck with an air-ride system installed to minimize the vibration during motion and a generator was carried

105 in the bed of the truck to provide electrical power. The inlet box was positioned above the front bumper of the vehicle,
forward of the generator and truck exhaust, to avoid self-sampling during mobile measurements (Fig. S1).
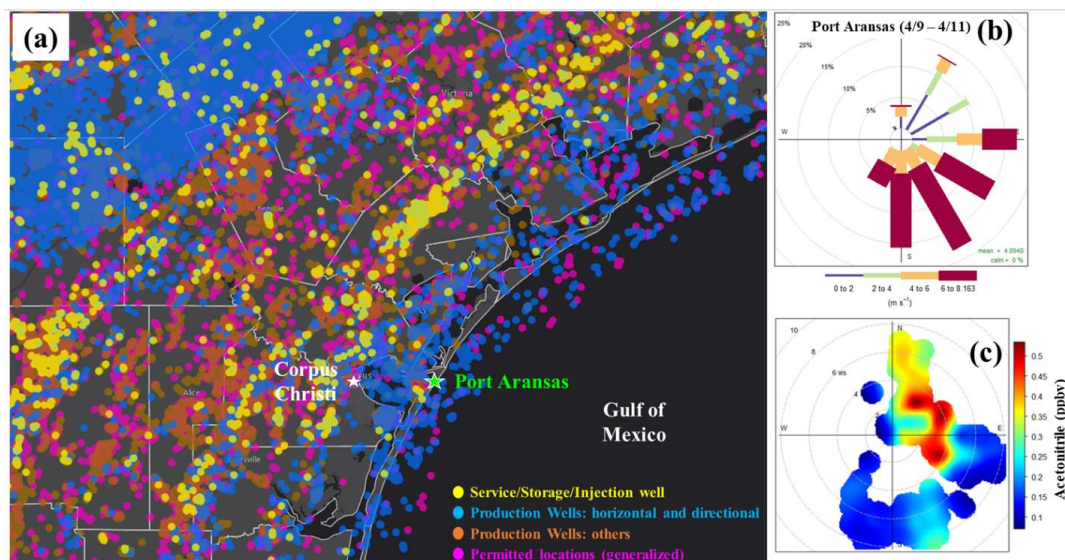
Figure 1. (a) GIS map of oil and gas activities in Texas (study site, PA is shown by green star)[1], **(b)** wind rose for PA
and **(c)** pollution rose plot for acetonitrile during the period of interest (4/9/2021 – 4/11/2021). The GIS map in panel
110 a was obtained from maps.fractracker.org (latest as of 05/08/2021).

2.2. Instrumentation

2.2.1. Aerosol optical parameters

The aerosol light absorption coefficient (σ_{abs}) was measured with a 3λ tricolor absorption photometer (TAP, Brechtel
Inc., Hayward, CA) at wavelengths of 365, 520, and 640 nm. The TAP is the commercially available version of the
115 National Oceanic and Atmospheric Administration (NOAA's) continuous light absorption photometer (CLAP) (Ogren
et al., 2017). The TAP consecutively samples through eight sample filter spots and two reference filter spots. During
deployment at PA, the TAP was set to rotate to the next filter spot when a filter spot's transmission reached 50 %.
The light scattering coefficient (σ_{scat}) was measured using an integrating nephelometer (model 3563, TSI Inc.,
Shoreview, MN) at wavelengths of 450, 550, and 700 nm. During the campaign the TSI nephelometer was calibrated
120 against zero air and carbon dioxide (CO_2) (Anderson and Ogren, 1998). The measured values were corrected for
angular scattering and truncation error (Anderson and Ogren, 1998; Bond et al., 2009) using the relationship: $\sigma_{corrected}$
= correction factor (C) × σ_{neph} where C is the correction factor, σ_{neph} is the scattering coefficient reported by the
instrument, and $\sigma_{corrected}$ is the corrected scattering coefficient (Shrestha et al., 2018). The correction factor (C) was

calculated using the Eq. (1) where the values for constants a and b were obtained from Anderson and Ogren (1998)
125 and SAE was calculated from the scattering coefficients measured during this study.

$$C = a + b * SAE^{\frac{\lambda 1}{\lambda 2}} \qquad (1)$$

Using 5-min averages, AAE and SAE were calculated as the negative slope of the linear fit of the optical parameter versus wavelength on a log-log plot (Bergstrom et al., 2007; Bond and Bergstrom, 2006; Kirchstetter et al., 2004). AAE and SAE provide information about the wavelength-dependence of absorption and scattering, respectively
130 (Schmeisser et al., 2017). Generally, AAE values of approximately 1 characterize fresh BC, whereas, BrC and mineral oxides show strong preferential light absorption in the UV range resulting in an enhancement in AAE values with respect to BC (Bond and Bergstrom, 2006; Bergstrom et al., 2007). SAE values are inversely related to the particle size distribution within the measured sample, so that generally SAE values less than 1 indicate size distribution dominated by coarser particles while those greater than 1 indicate that finer particles dominated the scattering aerosol
135 (Schuster et al., 2006). In this study, AAE above 1.2 (i.e. average AAE during non-BB influenced period + two times standard deviation) is used to indicate the periods of BB influence (discussed in Section 3.3.1). This threshold is used to identify events that lie above the baseline AAE for a given site.

Single Scattering Albedo (SSA) is the ratio of σ_{scat} to extinction coefficient ($\sigma_{scat} + \sigma_{abs}$), which provides information about the absorbing or scattering nature of the sampled aerosol. An SSA value greater than 0.95 represents aerosol
140 with a net cooling effect, while a value less than 0.85 will results in net warming. The SSA values between 0.85 and 0.95 may represent warming or cooling effect depending upon surface albedo and cloud cover (Ramanathan et al., 2001). The wavelengths for σ_{scat} and σ_{abs} were not the same, so to calculate SSA at 550 nm, the σ_{abs} measured at 540 nm was converted to that applicable to 550 nm using equation below:

$$\sigma_{abs}^{550} = \sigma_{abs}^{540} \times \left(\frac{\lambda_{540}}{\lambda_{550}}\right)^{AAE_{365-640}} \qquad (2)$$

145 **2.2.2. PM$_{2.5}$ filter sampling**

PM$_{2.5}$ samples were collected on 90-mm diameter quartz fiber filters (Pall Corporation, Port Washington, NY, USA) using a medium-volume (90 L min^{-1}; URG Corporation, Chapel Hill, North Carolina, USA) sampler at the Texas A&M Corpus Christi campus. Detailed discussion regarding filter collection protocols is reported in Yoon et al. (2021). We calculated equivalent black carbon (eBC) mass concentrations from the absorption coefficient measured
150 by TAP at a wavelength of 520 nm using mass absorption cross-section (MAC) values determined from the PM$_{2.5}$ filter samples. Details about the eBC calculation are presented in the *Supplementary Section S1*.

2.2.3. Real-time, size-resolved aerosol composition

An Aerodyne (Billerica, MA, USA) HR-ToF-AMS was used for size-resolved chemical characterization of non-refractory submicron aerosols (NR-PM$_1$) (DeCarlo et al., 2006). Detailed discussion regarding HR-ToF-AMS
155 operation and data handling followed during this study can be found in our previous publication (Zhou et al., 2023).

In brief, the size-resolved NR-PM$_1$ mass concentration and chemical composition were analyzed using the standard HR-ToF-AMS data analysis toolkit (SQUIRREL v1.64 and PIKA v1.24). Table S2 listed the MDLs of the five HR-ToF-AMS species (organic, sulfate, nitrate, ammonium, and chloride). Positive matrix factorization (PMF) analysis on the combined spectral matrices of organic and inorganic species of the HR-ToF-AMS (Zhou et al., 2017; Paatero and Tapper, 1994) identified seven organic aerosol (OA) factors associated with distinct sources and chemical and physical properties, which includes i) hydrocarbon-like OA (HOA) associated with traffic emissions, ii) biomass burning OA (BBOA), iii) less-oxidized oxygenated OA (LO-OOA) likely representing fresher secondary OA (SOA), iv) more-oxidized OOA (MO-OOA) likely representing more aged and processed SOA, v) less oxidized OOA that was associated with ammonium nitrate (AN-OOA), vi) highly oxidized OOA associated with ammonium sulfate (AS-OOA), and vii) highly oxidized OOA associated with acidic sulfate (acidic-OOA). Further, the f$_{60}$ value (i.e., the fraction of the signal at m/z 60 (mostly $C_2H_4O_2^+$) in the OA spectrum) above 0.3 % were used as markers for BB emissions (Docherty et al., 2008; Cubison et al., 2011).

2.2.4. Trace Gases and meteorological data

Nitric oxide (NO), nitrogen dioxide (NO$_2$), nitrogen oxides (NO$_x$ = NO + NO$_2$), total reactive nitrogen (NO$_y$), CO and O$_3$ were measured during the campaign. O$_3$ was monitored using a Thermo Environmental, Inc., Model 42C that has been modified to measure O$_3$ via chemiluminescence (CL) with NO gas. NO and NO$_2$ were measured using a CL instruments (Air Quality Design (Golden, CO)). The NO$_y$ was measured with a molybdenum oxide catalytic converter inlet and subsequent CL NO$_x$ analyzer. The CO was measured using off-axis integrated cavity output spectroscopy (Los Gatos Research, Inc., Li-7000). Greater detail about trace gas measurements are presented in our previous publications (Shrestha et al., 2022; Guo et al., 2021). The MDL and uncertainty for trace gas measurements during the campaign are presented in Table S3.

Basic meteorological parameters, including wind speed and direction, temperature and relative humidity, were measured continuously using RM Young 86000 ultrasonic anemometer. Fig. 1b shows that southeast wind was dominant at PA with intermittent wind from other directions during the campaign.

2.2.5. Volatile Organic Compounds (VOC)

A quadrupole proton transfer reaction- mass spectrometer (PTR-MS Q300; Ionicon Analytik, Austria) was used to measure VOCs during this study. In the PTR-MS, target gas molecules are ionized by proton transfer from protonated water (H$_3$O$^+$). The ionized material is then detected and quantified using a quadrupole mass spectrometer. A more detailed description of the PTR-MS is given in other studies (Lindinger and Jordan, 1998; de Gouw et al., 2003b; de Gouw and Warneke, 2007). A sample drying system similar to that used by Jobson and McCoskey (2010) was implemented to reduce any effects of water vapor that can occur with operating the PTR-MS at a lower E/N (100 Td). Greater details regarding PTR-MS operation, calibration and VOC data analysis followed in this study are presented

in our previous publication (Shrestha et al., 2022). The MDLs and uncertainty of the measured VOCs during the campaign are presented in Table S4.

2.3. Satellite observations
2.3.1. Active fire count and AOD

The ground-based measurements have been supported by the analysis of satellite aerosol optical depth (AOD) data obtained from the Moderate Resolution Imaging Spectroradiometer (MODIS), mounted onboard the Aqua and Terra satellites. The MODIS AOD gridded at a 10 x 10 km spatial was averaged for each day. This study uses level 3 AOD at 550 nm over land and ocean product for understanding trends in smoke aerosol loading (Remer et al., 2005; Levy et al., 2007).

Information about the daily active fires was obtained from the Visible Infrared Imaging Radiometer Suite (VIIRS) satellite observations. The VIIRS imagery-resolution bands sense 32, 375 m-pixel lines per scan with a field view of 112.56° (Li et al., 2020; Cao et al., 2014; Wolfe et al., 2013). The active fire confidence values below 70 % were eliminated during the data processing.

2.3.2. Satellite imagery of smoke plumes

The smoke map generated by NOAA Hazard Mapping System (HMS) was used to understand the spatial distribution of visible smoke plumes across North America. The NOAA HMS graphics system is an interactive satellite image developed by the National Environmental Satellite, Data, and Information Service (NESDIS). The satellite imagery can be downloaded from the NOAA smoke product website (https://satepsanone.nesdis.noaa.gov/FIRE/fire.html). These maps provide daily information on the horizontal distribution and density of the smoke plumes in the region (Rogers et al., 2020; Rolph et al., 2009; Fischer et al., 2018).

2.4. Backward trajectory analysis

The NOAA HYSPLIT model (Draxler and Hess, 1998; Stein et al., 2015) was used to simulate 72-h backward trajectories (BTs) at different starting heights (50, 100 and 500 m) every hour from April 9 through April 12, 2021 (CDT) at the PA site. The BTs at all three starting heights reported similar results; therefore, we chose the 50-m starting height for further analysis (Fig. S4). The HYSPLIT model has been used extensively for atmospheric transport and dispersion research in the last three decades. In this study, the HYSPLIT model was used to study possible source regions and estimate the age of the air masses arriving at the study site during the BB events. Meteorological data from the Global Data Assimilation System (GDAS) with $0.5° \times 0.5°$ spatial resolution were used in this study.

3. Result and discussion

During the stationary period when the MAQL2 was deployed in PA for the CCSA study, potential BB events were identified, first through the daily NOAA HMS updates of smoke across the Gulf and in the greater Corpus Christi area and then through evaluation of in-situ measurements of aerosols, VOCs and trace gas from the MAQL2. Two BB events were identified on April 10 (11:00 – 23:00 CST) and April 11 (6:45 – 14:00 CST) at PA and are referred as BB1 (orange shade) and BB2 (pink shade) hereafter (Fig. 2). The two BB events were first distinguished based on the observed pattern of enhancement in AAE and the HR-ToF-AMS tracer, f_{60} (*Section 3.1*); the accuracy of the AAE identification of BB influence was assessed in comparison with f_{60}. To better understand transport times and potential plume age, we analyzed possible source regions using BTs and satellite observations *(Section 3.2)*. Based on these results, we considered aerosol chemical speciation of NR-PM$_1$ (*Section 3.3*) and evaluated the efficacy of gas-phase BB tracers (including CO and acetonitrile) in an industrialized urban environment (*Section 3.4*). Finally, we discuss the potential implications of this BB event on Texas urban air quality.

3.1. Identifying biomass burning using aerosol optical properties

The aerosol optical, aerosol chemical speciation, trace gases and meteorological measurements from PA highlight changes in composition during the April 9-11 period of interest; this includes the day prior to the identified BB event. Based on the direction of the surface wind, the in-situ measurements were separated into marine and continental periods, while the BB designation was defined by the aerosol indicators (AAE and f60). (AAE and f_{60}). The measurement statistics during BB1, BB2, marine background and continental airmass periods are presented in Table 1. The short-duration events associated with local combustion that impact AAE and f_{60} values were removed from the marine average (see Fig. 2). Note that the statistics presented in this study are for a short period of interest (April 9 - 11) within a total campaign (April 3 -15), so the averages presented here differ from campaign averages reported in Zhou et al. (2023).

The σ_{abs} values for the ultraviolet-visible range (365-640 nm) were significantly higher during BB1 and BB2 (e.g., 5.57 ± 2.56 and 6.89 ± 2.42 Mm^{-1}, respectively, at 520 nm) compared to marine and continental airmasses (2.79 ± 1.16 and 4.12 ± 1.31 Mm^{-1}, respectively, at 520 nm) in the same week. However, the average σ_{scat} in all three wavelengths (450 nm, 550 nm and 700 nm) at PA were similar between BB and background marine airmass (Table 1). This does not agree with the studies conducted at remote locations and during airborne measurements of relatively fresh plumes that reported enhancement in aerosol scattering, mass concentration and number concentration during atmospheric transport of BB aerosols (Laing et al., 2020; Yokelson et al., 2009; Hobbs et al., 2003). It is interesting that the mean background σ_{scat} and σ_{abs} (56.52 Mm^{-1} and 2.79 Mm^{-1}) at PA were higher than some of the other coastal locations in the US such as Trinidad Head (σ_{scat} = 21.51 Mm^{-1} and σ_{abs} = 0.94 Mm^{-1}) and Pt. Reyes in California (σ_{scat} = 40 Mm^{-1} and σ_{abs} = 0.69 Mm^{-1}) and Cape Cod in Massachusetts (σ_{scat} = 16.08 Mm^{-1} and σ_{abs} = 1.10 Mm^{-1}) (Oltmans et al., 2008; Berkowitz et al., 2005; Titos et al., 2014). The higher background σ_{scat} and σ_{abs} at PA demonstrate the influence of anthropogenic emissions including shipping activities and oil and gas extraction on background aerosol in the Gulf of Mexico (Zhou et al., 2023).

The enhancement in σ_{abs} during the BB events was higher in the UV wavelength compared to longer wavelengths (Table 1). This wavelength dependency in aerosol absorption resulted in high AAE during BB1 and BB2 (1.2 ± 0.2 and 1.3 ± 0.2, respectively) compared to the marine (0.66 ± 0.14) and continental airmasses (0.94 ± 0.24) (Fig. 2a). The marine airmasses had AAE significantly less than 1, similar to other coastal locations such as Graciosa Island in Azores, Portugal (average AAE of 0.65) (Jefferson, 2010) and Pt. Reyes in California, USA (average of ~0.5) (Berkowitz et al., 2005; Schmeisser et al., 2017). The continental airmasses at PA during this study had AAE ~1, which is routinely reported in urban aerosols that contain BC from the fossil fuel combustion. Ambient aerosols impacted by BB can include brown carbon (BrC), which preferentially absorbs at lower wavelengths, resulting in an increased AAE (in excess of 2) (Bergstrom et al., 2007; Bond and Bergstrom, 2006; Kirchstetter et al., 2004). However, laboratory and field-based studies have reported a wide range of AAE values for different biomass fuel and burn conditions (0.55 to more than 3) (Gyawali et al., 2009; Bahadur et al., 2012; Pokhrel et al., 2016; Kirchstetter et al., 2004). Additionally, as the BrC emitted during wildfires decays during atmospheric transport (Forrister et al., 2015; Liu et al., 2016), there may be a subsequent decrease in AAE of the plume aerosols due to photobleaching (Reid et al., 2005; Eck et al., 2001; O'Neill et al., 2002). When considering the decrease during transport and dilution associated with mixing with local aerosol, it is not unexpected that the AAE during BB1 and BB2 at PA showed only a minor enhancement above the marine and continental backgrounds. In fact, similar AAE values have been reported for transported BB plumes impacting urban locations during South African (Bergstrom et al., 2007) and Yucatan fires (Marley et al., 2009). Although the AAE was impacted by the BB event, the SAE was consistent (1.5 - 1.7) during the period of interest. Locations that are influenced by coarse marine mode aerosols exhibit lower SAE (less than 1) (Costabile et al., 2013; Pandolfi et al., 2018; Titos et al., 2014). However, the slightly higher range of SAE observed at PA indicated additional influence of local anthropogenic emissions besides marine influence at the sampling site in PA (Zhou et al., 2023).

BB1 and BB2 events had clear synoptic peaks of eBC, OA and f_{60} (Fig 2 b & c). Both the eBC and OA concentrations were significantly enhanced during BB1 and BB2 while the f_{60} was 0.35 ± 0.12 % and 0.42 ± 0.10 % during BB1 and BB2 (Table 1). An f_{60} value above 0.3% indicates BB influence (Zhou et al., 2017). Thus, the aerosol BB tracers have good agreement with respect to the BB designation during the period of interest. However, the trace gas and eBC reveal a more complicated scenario. There was a good correlation for eBC with CO ($r^2 = 0.62$) and f_{60} ($r^2 = 0.75$) during BB2 and poor correlation with CO ($r^2 = 0.23$) and f_{60} ($r^2 = 0.27$) during BB1 (Figs. S2 & S3). Fig. 3 a-c shows that the patterns of AAE, f_{60}, eBC and CO were different during BB1 and BB2. The more specific BB tracers (AAE and f_{60}) had a different temporal trend than the more general combustion tracers (eBC and CO), indicating that PA was influenced by more than one type of combustion plume during BB1 and BB2. The high variability of the eBC and CO concentrations during BB1 is possibly driven by mixed plumes from different sources. Further, CO had high peaks for a couple of hours (18:00 – 20:00 CST) during BB1 when the wind speed was very low (~1 m s^{-1}). We assume that the high CO during that period was contributed by local non-BB combustion sources as indicated by elevated HOA concentrations (e.g. traffic or other primary combustion emissions), a lack of enhancement in acetonitrile concentration (discussed in *Section 3.4*) and poor correlations of CO with eBC and f_{60}.
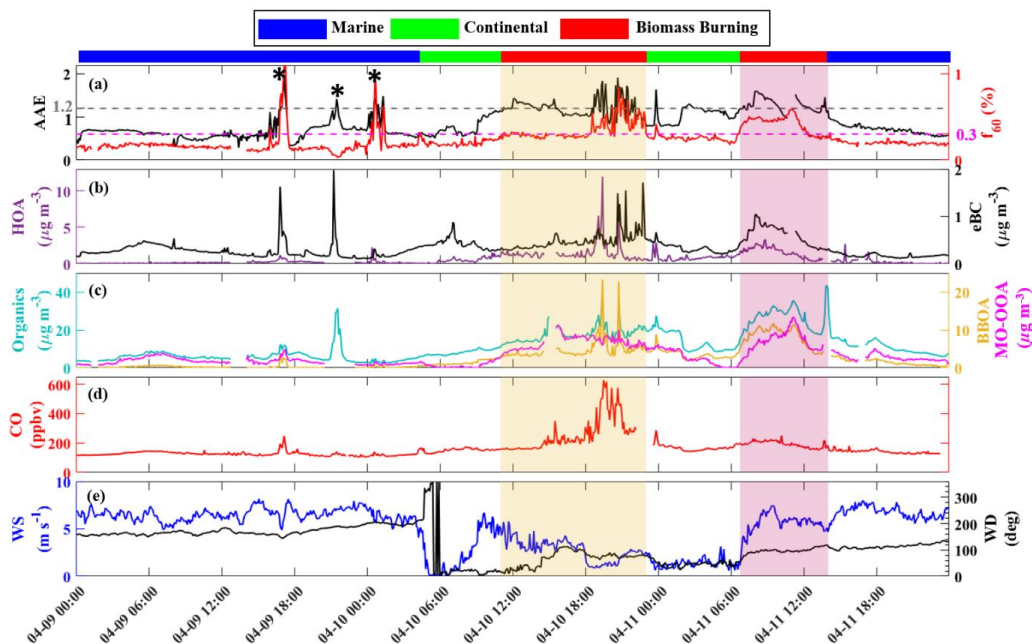
Figure 2. The marine and continental airmass classifications are differentiated based on the surface wind direction measured during the campaign. Time series plots for **(a)** AAE and f_{60} (dashed lines in grey and magenta represents AAE = 1.2 and f_{60} = 0.3 %, respectively) **(b)** HR-ToF-AMS HOA factor concentration, and eBC concentration, **(c)** OA, BBOA factor and MO-OOA factor concentrations **(d)** CO and **(e)** wind speed and direction. The short-duration events, indicated by the symbol * in panel **(a)**, associated with local combustion were removed from the marine average.

Table 1: Basic statistics (average ± standard deviation) of aerosol optical properties, aerosol speciation and select gases during the campaign. The short-duration events, indicated by the symbol * in Fig. 2a, associated with local combustion were removed from the marine average.

Parameters	BB1	BB2	Marine	Continental
σ_{abs} at 365 nm (Mm^{-1})	8.99 ± 4.52	11.5 ± 4.51	3.52 ± 1.49	5.81 ± 1.69
σ_{abs} at 520 nm (Mm^{-1})	5.57 ± 2.57	6.89 ± 2.42	2.79 ± 1.16	4.12 ± 1.31
σ_{abs} at 640 nm (Mm^{-1})	4.53 ± 2.05	5.53 ± 1.83	2.44 ± 1.02	3.49 ± 1.17
σ_{scat} at 450 nm (Mm^{-1})	64.9 ± 16.6	56.9 ± 12.7	73.3 ± 34.8	58.1 ± 36.2
σ_{scat} at 550 nm (Mm^{-1})	50.1 ± 15.0	41.2 ± 8.79	56.4 ± 26.8	43.2± 26.7
σ_{scat} at 700 nm (Mm^{-1})	34.2 ± 11.4	26.6 ± 5.34	37.4 ± 17.0	27.9 ± 16.9
AAE	1.21 ± 0.21	1.28 ± 0.16	0.66 ± 0.14	0.94 ± 0.24
SAE	1.52 ± 0.19	1.71 ± 0.10	1.55 ± 0.34	1.62 ± 0.19
SSA (550nm)	0.90 ± 0.02	0.87 ± 0.03	0.95 ± 0.03	0.90 ± 0.05

eBC (ng/m^3)	487 ± 224	601 ± 211	243 ± 102	359 ± 114
f_{60} (%)	0.35 ± 0.12	0.42 ± 0.10	0.17 ± 0.04	0.23 ± 0.04
OA ($\mu g/m^3$)	17.8 ± 4.81	26.4 ± 6.08	7.31 ± 3.93	11.3 ± 4.64
Acetonitrile (ppbv)	0.42 ± 0.10	0.18 ± 0.05	0.19 ± 0.07	0.27 ± 0.09
CO (ppbv)	259 ± 117	192 ± 21.7	130 ± 14.4	162 ± 20.2

300
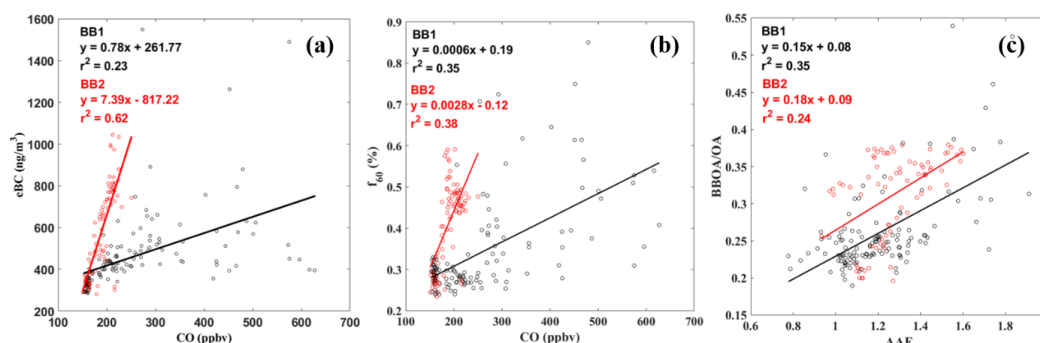
Figure 3. Correlation of **(a)** eBC versus CO **(b)** f_{60} versus CO and **(c)** BBOA/OA ratio versus AAE during BB1 and BB2. The slope of the regression lines in panel **(b)** is close to zero due to the difference in the magnitude of the f_{60} value and CO concentration.

3.2. Analysis of potential biomass burning source regions using satellite data and backward trajectory analysis

305   For this study, we evaluated MODIS AOD, VIIRS fire count, NOAA HMS smoke product, and HYSPLIT BTs to identify the fire source regions and estimate the plume age/transport times of BB1 and BB2, following a methodology similar to previous studies (Laing et al., 2016; Zhou et al., 2017; Deng et al., 2008; Mathur, 2008). The NOAA HMS smoke product indicated that PA had smoke in the column from April 10-16 (Fig. 4); however, it does not provide information about vertical distribution and boundary layer mixing of the smoke (Jaffe et al., 2020; Buysse et al., 2019).

310   Influence of BB on surface air quality was evident in the ground-based observations only on April 10 and 11 (see *Section 3.1*). Because we are most interested in the days with surface air quality impacts, we focused on source regions and transport during April 10-11. Extensive fire detects were evident in Central Mexico, the Yucatan peninsula, and the Central US during this period (Fig. 4). BTs ending at PA shifted gradually from Mexico to the Northern US over the course of the day on April 10 and remained from the Northern US through April 11 (Fig. S4), intersecting with

315   dense fire hotspots in the Central US (Oklahoma and Kansas). The air parcel heights during BB1 and BB2 were generally below 1500 meters above ground level (m.a.g.l.) when they passed over the active fire locations in the Central US (Fig. 4). As discussed above, the HMS smoke product indicated a smoke plume extending from Mexico, over the Gulf of Mexico, and to PA on both days during BB1 and BB2, indicating the possibility of influence of the fires in the Mexican region, which complicates the assignment of a specific source region. The smoke cover in the

320 Gulf of Mexico resulted in higher AOD values (0.5 ± 0.1; white square region in Fig. 4) on April 10 and 11 compared to the days prior to the event (0.3 ± 0.1), indicating heavy loading of aerosols on those days. Specifically, the MODIS grid that includes PA reported higher AOD during BB events (0.24) compared to the days prior to the event (0.18). Therefore, based on the BTs and satellite analysis, we assume that BB1 had mixed influence of transported smoke plumes from fires in Central Mexico, the Yucatan peninsula and the Central US, whereas BB2 was influenced

325 predominantly by fires in the Central US. Based on the combined information of fire hotspots and the BTs, we estimate that the transport time of smoke from the Mexican fires and the Central US fires ranged from 48-54 hours and 24-36 hours, respectively, before arriving at PA. The difference between the two BB events that was evident in the BB tracer analysis is then supported by differences in the BTs and source region analysis. The apparent local influence on CO and HOA is not specifically addressed by the satellite and BT analysis except to confirm that there were no local BB

330 sources immediately upwind of PA at this time. In a broad sense, these results highlight the importance of integrating ground-based monitors, including permanent in-situ air quality monitoring networks and intensive deployments, and satellite observations to understand the impact of smoke on surface air quality.
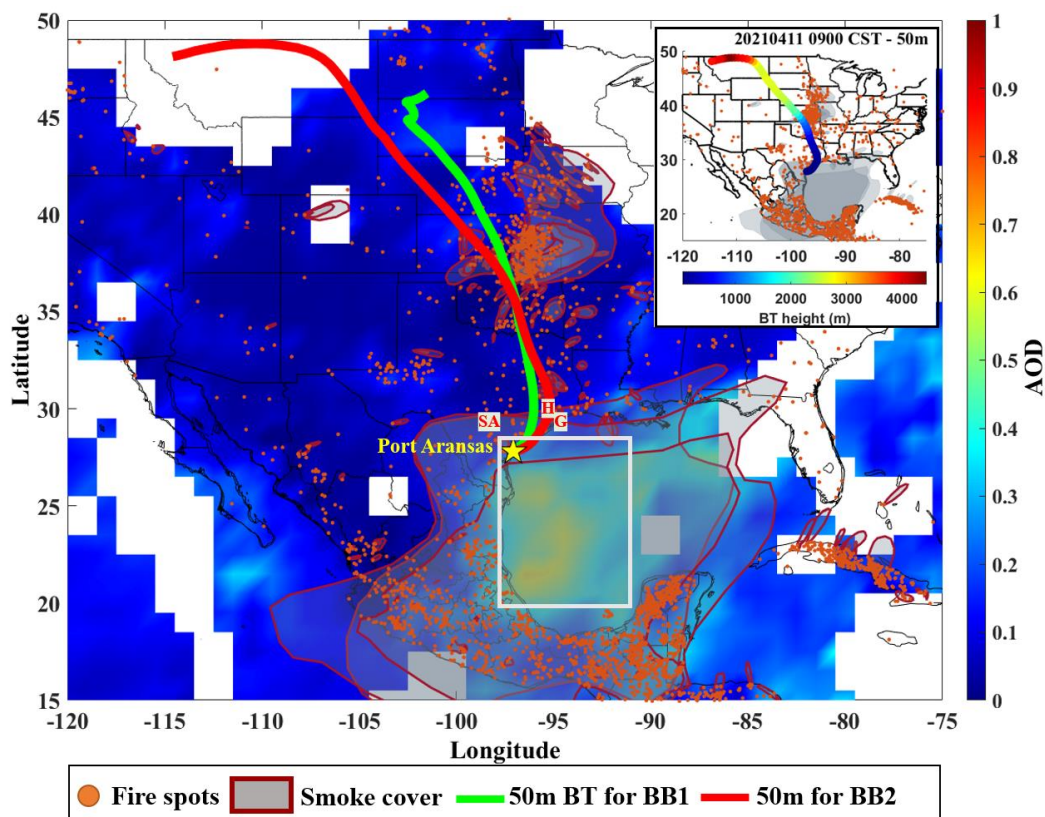
Figure 4. Spatial distribution of average AOD from Aqua and Terra satellites (April 10 – 11, 2021). The white outlined
335 box shows the grid size considered for calculating the average AOD. VIIRS active fire, NOAA HMS smoke and BTs are included in the main map and the inset. The inset plot also includes trajectory heights. The end times of the BTs

are chosen to represent the middle of the BB1 (4/10/21 20:00 CST) and BB2 (4/11/21 09:00 CST) observed in the ground-based measurement. The study site PA is denoted by a yellow star symbol. H, G and SA represents geolocations of other major cities in Texas (Houston, Galveston and San Antonio, respectively). This map was created in MATLAB.

3.3. Aerosol chemical composition during biomass burning events

To further characterize the two BB events at PA, we assessed the chemical speciation and the particle size-based OA composition from the HR-ToF-AMS. Figures 5 and S5 provide an overview of the aerosol composition from April 9-11. Differences in composition among marine background, continental and the two BB events are used here both to validate the BB designation and to further characterize the BB plume.

Previous studies have shown significant increase in NR-PM$_1$ concentration during BB events when the plumes are relatively fresh and the sampling locations do not have immediate anthropogenic sources (Zhou et al., 2017; Hu et al., 2016). In contrast, the average NR-PM$_1$ concentrations for this study were similar amongst BB1 (27.84 ± 6.53 µg/m^3), BB2 (33.96 ± 6.53 µg/m^3), marine background (27.59 ± 8.82 µg/m^3) and continental airmass (24.17 ± 9.42 µg/m^3). This result is similar to scattering coefficient measurements discussed in *Section 3.1*. These observations indicated that marine airmasses at PA were highly polluted with a submicron aerosol loading that included contributions from anthropogenic activities in the Gulf of Mexico (Zhou et al., 2023). Although the total NR-PM$_1$ concentrations were similar, the aerosol compositions changed drastically among the BB events, marine background and continental airmasses. During the BB events, organics dominated the aerosol composition (66 % and 78 % of NR-PM$_1$ during BB1 and BB2, respectively). The OA fraction was enhanced during BB1 and BB2 compared to the background marine (29 % of NR-PM$_1$) and continental airmasses (49 % of NR-PM$_1$). The OA fraction in the BB depends on the fuel burned and stage of fire (i.e., smoldering and flaming), and evolution during the transport. Generally, high values of OA fraction (greater than 90 %) have been reported for forest fires in the Amazon (Artaxo et al., 2013), North America (Kondo et al., 2011; Zhou et al., 2017) and Africa (Capes et al., 2008). Slightly lower OA fractions (~60-70 %) have been reported in Asia (Chakraborty et al., 2015; Kondo et al., 2011). Notably, the OA fractions observed during the BB events during this study are comparable to that reported for Yucatan fires (60 ± 11 %) (Yokelson et al., 2009). We assume that the lower range of OA fraction in this study is due to boundary layer mixing of the BB plume with local emissions and ageing during transport, as evidenced by the NR-PM$_1$ composition.

The background marine NR-PM$_1$ was dominated by sulfate (SO$_4$; 58 % of the total NR-PM$_1$ mass) whereas, the SO$_4$ fraction was second most prevalent constituent of continental airmass (38 % of the total NR-PM$_1$ mass), just slightly lower than the organic fraction (46 % of the total NR-PM$_1$ mass). The SO$_4$ fraction of NR-PM$_1$ was significantly lower during BB1 (23.07 ± 3.96 %) and BB2 (14.27 ± 7.32 %) but was still higher than in previous studies from Yucatan (0.89 ± 0.56 %) and Amazon fires (1.95 ± 0.83 %) (Yokelson et al., 2009; Ferek et al., 1998). The forest fires in this region are not a significant source of sulfate aerosol (Collier et al., 2016; Zhou et al., 2017; Yokelson et al., 2009). Zhou et al. (2023) reported that anthropogenic sulfate remained the dominant sulfate source in the Gulf, coastal, and continental airmasses during the same study, whereas mass concentrations of sea-salt sulfate and biogenic sulfate were

the largest in the Gulf air masses and decreased with increasing continental influences. These results from Zhou et al. (2023) highlighted anthropogenic shipping emissions over the Gulf of Mexico as a major contributor to sulfate at PA during the campaign.

375   The nitrate fraction of NR-PM$_1$ was similar during BB1 (8 %) and BB2 (5 %). Studies have confirmed that particulate organonitrates (ON) in the atmosphere are closely associated with BB emissions (Joo et al., 2019; Brege et al., 2018; Zhu et al., 2021; Tiitta et al., 2016). In this study, ON were observed and appeared to account for most of the NO$^+$ and NO$_2^+$ (major ions of inorganic and organic nitrates in HR-ToF-AMS) signals detected in NR-PM$_1$ during the BB periods. The signal ratios of NO$^+$ and NO$_2^+$ were 7.5 and 7.7 for BB1 and BB2, respectively, substantially higher than

380   the ratio for pure ammonium nitrate particles (R$_{AN}$ = 2.38). Based on this information and following the method proposed by Farmer et al. (2010), we estimate that nearly all the NO$^+$ and NO$_2^+$ signals measured during the BB periods (~92% and ~99% for BB1 and BB2, respectively) were contributed by ON. This ON may have contributed to the increase in AAE during BB1 and BB2. Thus, we observe potential indication of BrC as represented by ON.

The PMF analysis of NR-PM$_1$ can facilitate our characterization of the two different BB events (Figure 2 and S5).

385   Using both the specific tracers, AAE and f$_{60}$, in addition to the PMF results, we see interesting differences between BB1 and BB2. Although AAE, f$_{60}$, CO, and BBOA generally increase during BB1 and BB2, the period from 18:00 – 22:00 on April 10 does not have good agreement among the tracers. The HOA and BBOA factors had good correlation (r^2= 0.79) during BB1 (Fig. S2), but the BBOA factor did not follow same trend as the AAE and f$_{60}$ this short time period. The HOA factor is mostly associated with fresh or local combustion sources and more closely mimics the CO trends (discussed in *Section 3.1*) during the time period of BB1, which may again hint that the extreme CO peak in

390   the evening of April 10 was a local combustion source not of BB origin. Interestingly, the MO-OOA factor mirrors some of the more gradual increase seen in the AAE and f$_{60}$ but does not include any of the sharp increases. Laboratory experiments and field observations have shown that the mass spectrum of OA from BB becomes increasingly like MO-OOA as it photochemically ages (Hennigan et al., 2011; Grieshop et al., 2009; Zhou et al., 2017). Therefore, MO-OOA factor can increase as OA from BB emissions ages and act as an indicator of aging of BB aerosols (Bougiatioti

395   et al., 2014). For BB2, all the BB tracers (AAE, f$_{60}$, BBOA, MO-OOA, CO, and eBC) are in good agreement. It seems that for these BB events, both BBOA and MO-OOA factors are needed to clearly describe the two plumes, while the HOA, CO and AAE facilitate the disentangling of the mixed combustion signal for BB1.

The eight ion families at m/z < 120 (in different colors) and the elemental ratio of bulk OA (O/C, H/C, N/C and

400   OM/OC) during BB1 and BB2 are included in Fig. S5. During BB1 and BB2, O/C, H/C and OM/OC were similar (O/C = 0.53 and 0.58, H/C= 1.37 and 1.34, and OM/OC= 1.84 and 1.90, respectively). Generally, O/C ratio ≥ 0.6 and H:C ratio ≥ 1.2 represent highly oxidized and highly saturated airmass (Brito et al., 2014; Brege et al., 2018; Tu et al., 2016; Zhou et al., 2017). Therefore, the observed elemental ratios during BB1 and BB2 in this study tend to agree well with the processed or oxidized airmass as reported in aged smoke plumes. Also, as evident in the MO-OOA

405   factor, the consistency in elemental ratios between BB1 and BB2 shows that, regardless of the material burned, aerosols become chemically identical as they age and smoke plume gets more diluted (Jimenez et al., 2009; Ng et al., 2010; Brito et al., 2014). Specific fragments can improve understanding of differences in OA composition and processing during BB1 and BB2, f$_{44}$ vs. f$_{43}$ (Fig. S5i) and f$_{44}$ vs. f$_{60}$ (Fig. S5j) plots are included in the supplemental

information (Ng et al., 2010; Cubison et al., 2011). The average f_{44} values for BB1 (0.17) and BB2 (0.16) were similar, but BB2 had slightly higher f_{43} than BB1 (0.059 vs. 0.051), which is consistent with BB2 being primarily composed of an aged BB plume. The two BB events generally overlapped on the f_{44} vs. f_{60} space. The progression of f_{44} vs. f_{43} and f_{44} vs. f_{60} as a function of time elapsed during BB2 are also shown in Fig. S5 (i-j). The observed direction of the trend during BB2 was similar to previous field studies, showing increase in f_{44} and reduction in f_{60} due to photochemical aging (Cubison et al., 2011). Previous studies have shown that increase in f_{44} with photochemical aging may lead to the production of carboxylic acids (Zhang et al., 2005; Takegawa et al., 2007). There was not a discernible temporal progression in these relationships for BB1.

Figure 5 (b-c & e-f) shows the average size distributions and chemical compositions of NR-PM$_1$ and the size distribution of key organic mass fragments (m/z 43, 44, 55, 57 and 60) during BB1 and BB2. The m/z 43 and 44 were dominated by $C_2H_3O^+$, an ion fragment from oxidized organic compounds including aldehydes and ketones, and CO_2^+, an ion fragment from carboxylic acids, whereas, m/z 55 and 57 were dominated by $C_4H_7^+$ and $C_4H_9^+$, respectively, which are ion fragments from hydrocarbons. The m/z 60 was primarily the AMS BB indicator, $C_2H_4O_2^+$, ion fragment of anhydrous sugar (e.g., levoglucosan). During BB2, the aerosol composition and the organic fragments showed a unimodal distribution, with a mode diameter in the accumulation mode size range of about 400 nm; the aerosol appears to be internally mixed. This confirms our previous discussion that the oxidized organic compounds ubiquitously dominated the aerosols during BB2, signifying the presence of aged BB emissions (Alfarra et al., 2004; Zhang et al., 2005; Chakraborty et al., 2015). During BB1, the size distribution of total nitrates, OA and organic mass fragments showed a similar distribution peaking at about 400 nm. However, the size distribution of sulfate and ammonium aerosols showed peaks at a significantly larger diameter of about 700 nm, and m/z 60, 55, and 57 showed enhanced signals at condensation mode (~100 - 200 nm) compared to those during BB2. Given the difference in the size distribution of aerosol composition during BB1, it appears be externally mixed. The contribution of sulfate and ammonium to the NR-PM$_1$ composition for BB1 is also much greater than for BB2 (sum of 31 % and 19 %, respectively). The external mixing and the higher contribution of ammonium sulfate likely represents a mixture of organics from aged BB emission with an anthropogenic marine signal (e.g. inclusion of shipping activities and oil and gas extraction as discussed in earlier sections and in Zhou et al. (2023). This marine signal in BB1 may be indicating that the Mexican fires transported over the Gulf of Mexico contributed to BB1 while the internal mixing and lack of marine signal in BB2 may indicate that the Central US fires dominated that period. However, the presence of mixed sources of processed BB aerosols and non-BB anthropogenic emissions at PA complicates the size distributions of NR-PM$_1$ composition for both BB1 and BB2 events, which needs further investigation.
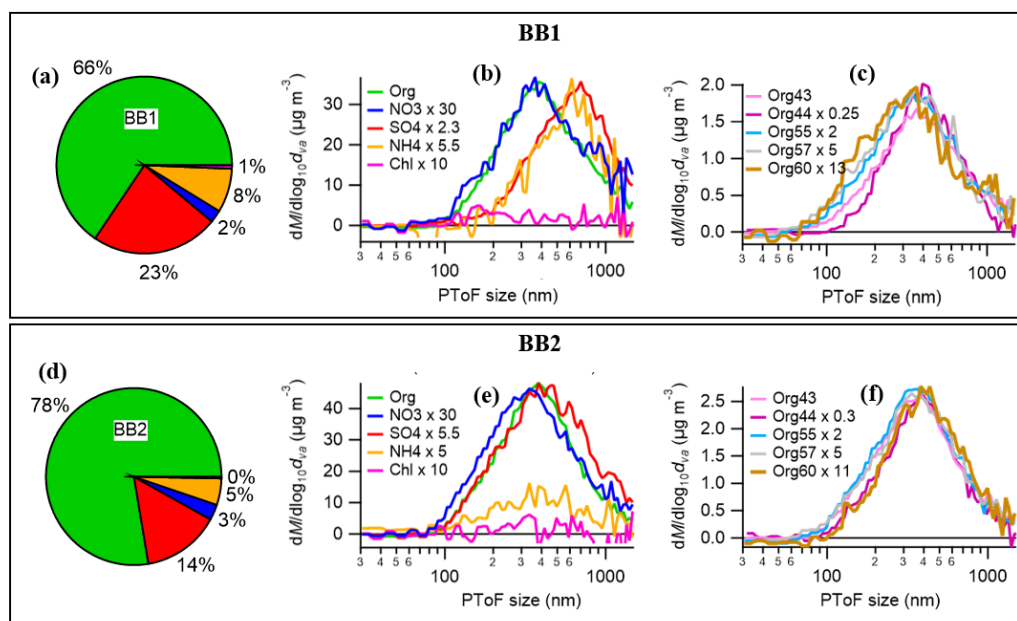
Figure 5. (a) Pie chart showing NR-PM$_1$ composition during BB1, **(b-c)** average particle time-of-flight (PToF) size distribution of NR-PM$_1$ species and select organic m/zs during BB1, **(d)** Pie chart showing NR-PM1 composition during BB2, **(e-f)** Average size distribution of NR-PM$_1$ species and select organic m/zs during BB2. In the pie-charts (panels a and d): organics (in green), nitrates (in blue), sulfates (in red), ammonium (in yellow) and chloride (in magenta).

3.4. Application of acetonitrile as VOC tracer for biomass burning

BB emissions consist of a mixture of organic and inorganic compounds in the gas and aerosol phase (Holzinger et al., 1999). As with the aerosol fraction, there are common VOC markers for BB; acetonitrile has been utilized as a BB tracer in PTR-MS measurements (de Gouw et al., 2003a; Karl et al., 2003; Sinha et al., 2014). BB emissions are a significant component of the global budget of acetonitrile (de Gouw et al., 2003a; Holzinger et al., 1999, 2001). However, studies have highlighted that acetonitrile signals from BB can be convoluted by local vehicular emissions (Guan et al., 2020; Swarthout et al., 2013), coal-burning (Jobson et al., 2010; Valach et al., 2014; Inomata et al., 2013) and industrial emissions including oil and gas activities (Cai et al., 2019). In fact, background acetonitrile levels have been reported to vary from ~100 pptv to above 600 pptv across different regions (Huangfu et al., 2021 and references therein). Therefore, using acetonitrile in an anthropogenically-influenced environment like PA requires careful consideration (Huangfu et al., 2021). In this section we evaluate the efficacy of acetonitrile as a BB tracer for dilute plumes on the Gulf Coast of Texas.

During the two BB events identified in this study, the acetonitrile did not follow the same trend as AAE or f$_{60}$ (Fig. 6a & Fig. 2). Acetonitrile had peaks prior to the onset of BB1 and in the early afternoon of April 10 with relatively low

concentrations during BB2. Thus, we hypothesize that the acetonitrile levels at the study site are impacted by emissions
460   from the dense network of on-shore and off-shore oil and gas activities in the PA/Corpus Christi region and/or urban
background during continental airmass regimes (Fig. 1c). To determine whether the acetonitrile mixing ratios
associated with the observed BB plumes at PA would exceed the local background, we (i) investigated the geospatial
variability of acetonitrile emissions (including industrial and traffic sources) in Corpus Christi by evaluating mobile
measurements and (ii) estimated the acetonitrile in the BB events using an enhancement ratio of CO with respect to
465   acetonitrile from the literature (Warneke et al., 2006).

The mobile measurement shows that while the ambient acetonitrile concentration varied on a daily basis, acetonitrile
concentration was clearly enhanced in the major industrial sector of Corpus Christi (Fig. 6). The acetonitrile
concentration in PA did not surpass the average measured acetonitrile from the major industrial sector of Corpus
Christi in either BB event (Fig. 6a). These results indicate that local anthropogenic emissions likely enhance the
470   background acetonitrile level in PA. Additional investigation is needed to characterize and define these local sources.
To further test acetonitrile as a BB tracer for this study, we estimated the BB-associated acetonitrile using an
orthogonal regression-based equation formulation by Warneke et al. (2006). Because we observed CO enhancement
during BB1 and BB2, we reorganized the equation to estimate acetonitrile concentration during the BB events (Eq.
(3) below). We acknowledge the limitation of this calculation which assumes: (i) the entire CO enhancement above
475   background is from the BB influence and (ii) 0.36 ppbv of CO per pptv of acetonitrile is observed in the BB plume in
an urban environment.

$$Estimated\ Acetonitrile = \left(\frac{Ambient\ CO-CO\ background}{ER_{CO-acetonitrile}} \right) - Acetonitrile\ background \qquad (3)$$

where CO background = 75 ppbv, Enhancement Ratio ($ER_{CO\text{-}acetonitrile}$) = 0.36 ppbv and acetonitrile background = 0.115
ppbv were used as reported in Warneke et al. (2006).

480   Fig. 6a shows a timeseries of ambient acetonitrile measured during the campaign and the estimated acetonitrile
concentration using the above-mentioned Eq. (3). The observed and estimated acetonitrile were similar during BB2,
indicating that the observed acetonitrile was potentially influenced by the BB2 plume. However, the estimated
acetonitrile did not match the observed acetonitrile during BB1 or during the preceding period of continental influence.
The observed acetonitrile was higher than estimated acetonitrile during the preceding period of continental influence,
485   likely indicating the local industrial sources of acetonitrile as mentioned above. However, in the evening of April 10,
the calculated acetonitrile was well above the ambient acetonitrile levels. This switch to conditions of estimated
acetonitrile greater than observed acetonitrile likely indicates a local combustion source that emits CO but does not
emit acetonitrile and is therefore likely not BB. This analysis highlights that both CO and acetonitrile can be impacted
by local sources and specifically that acetonitrile cannot be used as a unique BB tracer for dilute BB plumes when the
490   background acetonitrile level is high due to the presence of local anthropogenic sources. Besides acetonitrile, other
VOCs like furans, furfurals and hydrogen cyanide have also been used as the BB tracer (Tripathi et al., 2022; Coggon
et al., 2016; Bruns et al., 2017), however, the applicability of these VOCs could not be accessed in this study since
they were not included in the select list of measured compounds. Overall, this study demonstrates that AAE and
aerosol composition served as reliable indicators of transported BB plumes in urban environment.
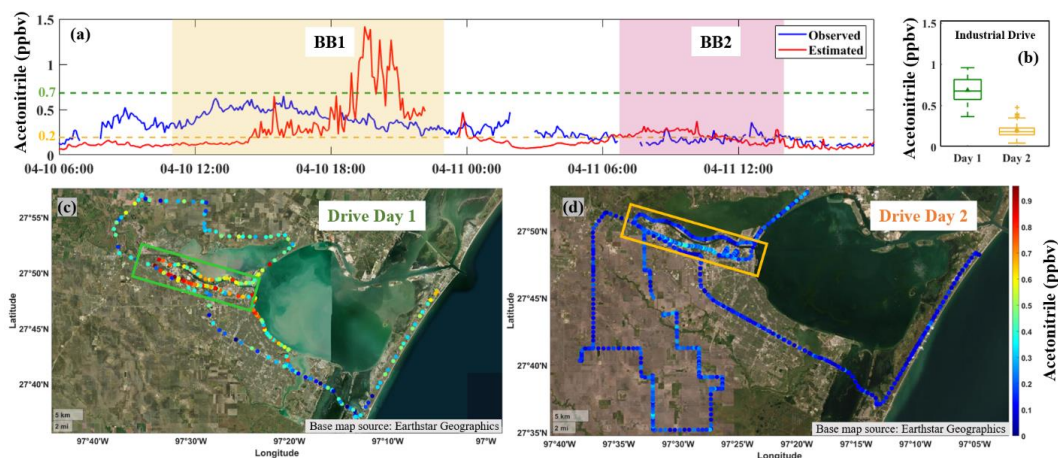
495

Figure 6. (a) Time series for ambient acetonitrile observed during the campaign (in blue) and estimated acetonitrile (in red color) using the reorganized equation from Warneke et al. (2006); **(b)** Box plot showing the acetonitrile concentration measured in the industrial corridor during mobile measurements on drive day 1 (April 16) and drive day 2 (April 18); and **(c-d)** acetonitrile concentration measured during mobile measurements on April 16 and 18 in Corpus

500 Christi. The location of major industrial corridor is marked by the green box (panel c) and orange box (panel d). The dashed lines in green and orange (panel a) represent average acetonitrile concentration measured in the major industrial corridor during drive days 1 and 2, respectively. The spatial distribution acetonitrile (panel c and d) were created in MATLAB.

4. Atmospheric Implication and Outlook

505 Previous studies have demonstrated that transported BB plumes advected to the surface can contribute to O_3 production and lead to exceedances of the National Ambient Air Quality Standard (NAAQS) (Wilkins et al., 2020; Schade et al., 2011; McMillan et al., 2010; Lei et al., 2018; Langford et al., 2015). For instance, transported BB emission was estimated to contribute ~10 ppbv to two O_3 exceedance days in Las Vegas during summer of 2013 (Langford et al., 2015). Similarly, Wilkins et al. (2020) asserted that aged BB plumes were more O_3 enriched and

510 reported that aged plumes (4 - 7 days) contributed, on average, 15 ppbv to surface O_3 in the Midwestern US. Lei et al. (2018), McMillan et al. (2010) and Schade et al. (2011) showed the transport of CO and O_3 from fires in the US Pacific Northwest to Houston, which then contributed to an O_3 exceedance period in the Houston area. These results highlight that BB contribution can be important factor in urban O_3 chemistry.

During the BB events discussed in this study, the Texas Commission on Environmental Quality (TCEQ) O_3 monitors

515 recorded elevated O_3 concentrations across Southern Texas. Figure 7a shows the time series of O_3 concentration for April 9-11 in Southern Texas including Houston-Galveston, San Antonio and Corpus Christi. Three representative sites from each of these metropolitan areas are plotted to highlight concurrent enhancement in O_3 on those days. There were more than thirty other TCEQ sites that showed elevated O_3 concentration above 65 ppbv during this time period

(https://www.tceq.texas.gov/gis/geotam-viewer). The presence of smoke in Houston can be evaluated using the Black

520 and Brown Carbon (BC)[2] network. (BC)[2] is a TCEQ-funded aerosol optical network in Texas operated by our research group that utilizes the same aerosol optical measurement instrumentation as in this study. Elevated AAE was also observed on April 10-12 at (BC)[2] in Houston (Fig. 7b). These results indicated that the smoke distribution from the NOAA HMS product (Fig. 4) may have had regional impacts on O_3 concentrations across Southern Texas. However, accurately estimating the contribution from BB emission to the local O_3 enhancement with single-point measurements

525 is difficult (Thompson et al., 2019). Additional investigation of this regional event is needed to confirm the potential BB contribution to urban air quality.

Permanent ground-based air quality monitoring networks play a crucial role in identifying such events but often lack specificity towards identification of BB influence. In this regard, the low-cost aerosol optical measurements in this study exhibited exceptional ability to identify BB events even in a dilute plume in an industrialized urban environment.

530 The results of this study support the implementation of an extended network of low-cost aerosol optical measurements to identify the influence of BB plumes, especially in cities that are designated as non-attainment or marginal nonattainment of criteria air pollutants.
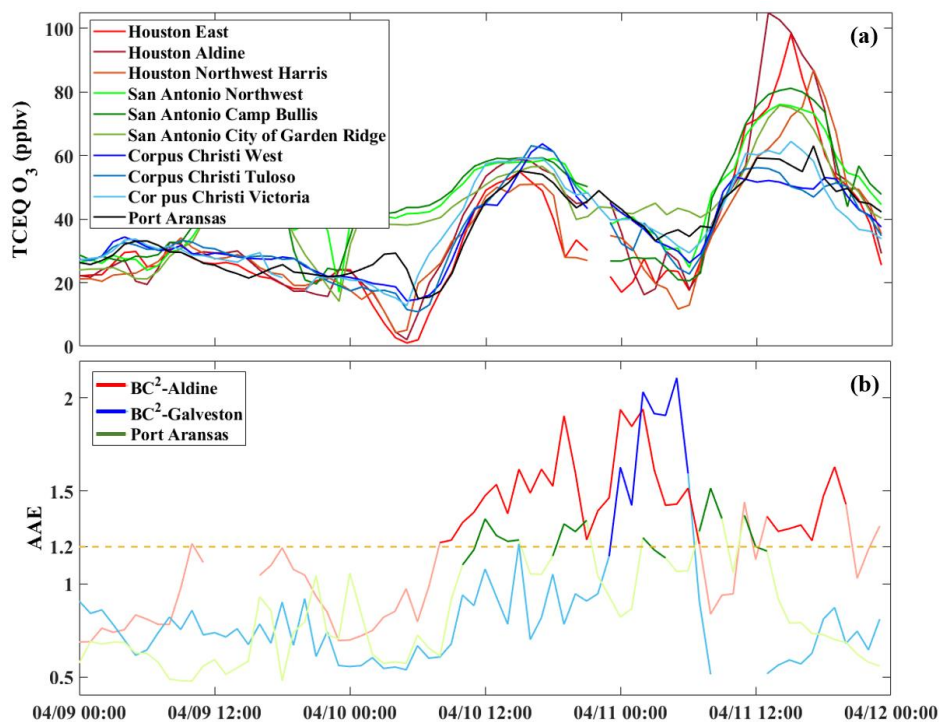
Fig. 7. Time series of **(a)** O_3 concentrations reported by TCEQ sites and PA (this study); **(b)** AAE observed at (BC)[2]-

535 sites in Houston and PA. AAE above the threshold for BB indication (campaign average + 2 standard deviation) is plotted in darker color. Hourly data from the different air quality monitors including O_3 from the TCEQ monitors are available from the TCEQ website (https://www.tceq.texas.gov/gis/geotam-viewer).

Data availability

540 The data used in this study can be accessed through the publicly available link: https://dataverse.tdl.org/privateurl.xhtml?token=b8358b91-39d6-4aa2-aa84-4b8383f278fd.

Author Contributions

SS, MM, MCG, SY, SA, SZ, FG, CYC, JHF, RJS, SU and RJS participated in the field campaign, including measurements and data quality assurance. S.S. performed data analysis. R.J.S. supervised the project and data analysis. S.S. prepared draft of the manuscript. S.S., and R.J.S. edited final version of the manuscript. All authors reviewed the 545 manuscript and provided inputs for data analysis.

Competing Interest

The authors declare that they have no conflict of interest.

Acknowledgements

We would like to thank Dr. J. David Felix of Texas A&M Corpus Christi for assistance with the filter sampling at 550 TAMU-CC and Jonathan White of Baylor University for assistance with the OCEC analysis. The preparation of this manuscript was financed through a grant from the Texas Commission on Environmental Quality (TCEQ, Grant number: 582-18-81339), administered by the University of Texas at Austin, Center for Energy and Environmental Resources (CEER) through the Air Quality Research Program (AQRP). The black and brown carbon $(BC)^2$ monitoring in Houston and El Paso in 2021 Ozone season was financed through the TCEQ (Grant number: 582-18-81339). The 555 content, findings, opinions, and conclusions are the work of the authors and do not necessarily represent findings, opinions, or conclusions of the TCEQ or the AQRP. The authors gratefully acknowledge the NOAA Air Resources Laboratory (ARL) for the provision of the HYSPLIT transport and dispersion model and/or READY website (http://www.ready.noaa.gov) used in this publication. The authors acknowledge FracTracer Alliance for the permission to use GIS map of oil and gas activities in Texas.

560 **References**

Alfarra, M. R., Coe, H., Allan, J. D., Bower, K. N., Boudries, H., Canagaratna, M. R., Jimenez, J. L., Jayne, J. T., Garforth, A. A., Li, S.-M., and Worsnop, D. R.: Characterization of urban and rural organic particulate in the Lower Fraser Valley using two Aerodyne Aerosol Mass Spectrometers, Atmos. Environ., 38, 5745–5758, https://doi.org/10.1016/j.atmosenv.2004.01.054, 2004.

565 Anderson, D. C., Pavelec, J., Daube, C., Herndon, S. C., Knighton, W. B., Lerner, B. M., Roscioli, J. R., Yacovitch, T. I., and Wood, E. C.: Characterization of ozone production in San Antonio, Texas, using measurements of total peroxy radicals, Atmos. Chem. Phys., 19, 2845–2860, https://doi.org/10.5194/acp-19-2845-2019, 2019.

Anderson, T. L. and Ogren, J. A.: Determining Aerosol Radiative Properties Using the TSI 3563 Integrating
Nephelometer, Aerosol Sci. Technol., 29, 57–69, https://doi.org/10.1080/02786829808965551, 1998.

570 Artaxo, P., Rizzo, L. V., Brito, J. F., Barbosa, H. M. J., Arana, A., Sena, E. T., Cirino, G. G., Bastos, W., Martin, S.
T., and Andreae, M. O.: Atmospheric aerosols in Amazonia and land use change: from natural biogenic to biomass
burning conditions, Faraday Discuss., 165, 203, https://doi.org/10.1039/c3fd00052d, 2013.

Bahadur, R., Praveen, P. S., Xu, Y., and Ramanathan, V.: Solar absorption by elemental and brown carbon
determined from spectral observations., Proc. Natl. Acad. Sci. U. S. A., 109, 17366–71,

575 https://doi.org/10.1073/pnas.1205910109, 2012.

Bein, K. J., Zhao, Y., Johnston, M. V., and Wexler, A. S.: Interactions between boreal wildfire and urban emissions,
J. Geophys. Res., 113, D07304, https://doi.org/10.1029/2007JD008910, 2008.

Bergstrom, R. W., Pilewskie, P., Russell, P. B., Redemann, J., Bond, T. C., Quinn, P. K., and Sierau, B.: Spectral
absorption properties of atmospheric aerosols, Atmos. Chem. Phys., 7, 5937–5943, https://doi.org/10.5194/acp-7-

580 5937-2007, 2007.

Berkowitz, C. M., Jobson, B. T. T., Alexander, M. L., Laskin, A., and Laulainen, N. S.: Aerosol Composition and
Morphology during the 2005 Marine Stratus Radiation Aerosol and Drizzle Study, in: American Geophysical Union,
Fall Meeting, 2005.

Bhattarai, H., Saikawa, E., Wan, X., Zhu, H., Ram, K., Gao, S., Kang, S., Zhang, Q., Zhang, Y., Wu, G., Wang, X.,

585 Kawamura, K., Fu, P., and Cong, Z.: Levoglucosan as a tracer of biomass burning: Recent progress and
perspectives, Atmos. Res., 220, 20–33, https://doi.org/10.1016/j.atmosres.2019.01.004, 2019.

Bond, T. C. and Bergstrom, R. W.: Light absorption by carbonaceous particles: An investigative review, Aerosol
Sci. Technol., 40, 27–67, https://doi.org/10.1080/02786820500421521, 2006.

Bond, T. C., Covert, D. S., and Müller, T.: Truncation and Angular-Scattering Corrections for Absorbing Aerosol in

590 the TSI 3563 Nephelometer, Aerosol Sci. Technol., 43, 866–871, https://doi.org/10.1080/02786820902998373,
2009.

Bougiatioti, A., Stavroulas, I., Kostenidou, E., Zarmpas, P., Theodosi, C., Kouvarakis, G., Canonaco, F., Prévôt, A.
S. H., Nenes, A., Pandis, S. N., and Mihalopoulos, N.: Processing of biomass-burning aerosol in the eastern
Mediterranean during summertime, Atmos. Chem. Phys., 14, 4793–4807, https://doi.org/10.5194/acp-14-4793-2014,

595 2014.

Brege, M., Paglione, M., Gilardoni, S., Decesari, S., Facchini, M. C., and Mazzoleni, L. R.: Molecular insights on
aging and aqueous-phase processing from ambient biomass burning emissions-influenced Po Valley fog and aerosol,
Atmos. Chem. Phys., 18, 13197–13214, https://doi.org/10.5194/acp-18-13197-2018, 2018.

Brito, J., Rizzo, L. V., Morgan, W. T., Coe, H., Johnson, B., Haywood, J., Longo, K., Freitas, S., Andreae, M. O.,

600 and Artaxo, P.: Ground-based aerosol characterization during the South American Biomass Burning Analysis
(SAMBBA) field experiment, Atmos. Chem. Phys., 14, 12069–12083, https://doi.org/10.5194/acp-14-12069-2014,
2014.

Bruns, E. A., Slowik, J. G., El Haddad, I., Kilic, D., Klein, F., Dommen, J., Temime-Roussel, B., Marchand, N.,
Baltensperger, U., and Prévôt, A. S. H.: Characterization of gas-phase organics using proton transfer reaction time-

605   of-flight mass spectrometry: fresh and aged residential wood combustion emissions, Atmos. Chem. Phys., 17, 705–720, https://doi.org/10.5194/acp-17-705-2017, 2017.

Buysse, C. E., Kaulfus, A., Nair, U., and Jaffe, D. A.: Relationships between Particulate Matter, Ozone, and Nitrogen Oxides during Urban Smoke Events in the Western US, Environ. Sci. Technol., 53, 12519–12528, https://doi.org/10.1021/acs.est.9b05241, 2019.

610   Cai, S., Zhu, L., Wang, S., Wisthaler, A., Li, Q., Jiang, J., and Hao, J.: Time-Resolved Intermediate-Volatility and Semivolatile Organic Compound Emissions from Household Coal Combustion in Northern China, Environ. Sci. Technol., 53, 9269–9278, https://doi.org/10.1021/acs.est.9b00734, 2019.

Cao, C., De Luccia, F. J., Xiong, X., Wolfe, R., and Weng, F.: Early On-Orbit Performance of the Visible Infrared Imaging Radiometer Suite Onboard the Suomi National Polar-Orbiting Partnership (S-NPP) Satellite, IEEE Trans.

615   Geosci. Remote Sens., 52, 1142–1156, https://doi.org/10.1109/TGRS.2013.2247768, 2014.

Capes, G., Johnson, B., McFiggans, G., Williams, P. I., Haywood, J., and Coe, H.: Aging of biomass burning aerosols over West Africa: Aircraft measurements of chemical composition, microphysical properties, and emission ratios, J. Geophys. Res., 113, D00C15, https://doi.org/10.1029/2008JD009845, 2008.

Chakraborty, A., Bhattu, D., Gupta, T., Tripathi, S. N., and Canagaratna, M. R.: Real-time measurements of ambient
620   aerosols in a polluted Indian city: Sources, characteristics, and processing of organic aerosols during foggy and nonfoggy periods, J. Geophys. Res. Atmos., 120, 9006–9019, https://doi.org/10.1002/2015JD023419, 2015.

Coggon, M. M., Veres, P. R., Yuan, B., Koss, A., Warneke, C., Gilman, J. B., Lerner, B. M., Peischl, J., Aikin, K. C., Stockwell, C. E., Hatch, L. E., Ryerson, T. B., Roberts, J. M., Yokelson, R. J., and de Gouw, J. A.: Emissions of nitrogen-containing organic compounds from the burning of herbaceous and arboraceous biomass: Fuel composition
625   dependence and the variability of commonly used nitrile tracers, Geophys. Res. Lett., 43, 9903–9912, https://doi.org/10.1002/2016GL070562, 2016.

Collier, S., Zhou, S., Onasch, T. B., Jaffe, D. A., Kleinman, L., Sedlacek, A. J., Briggs, N. L., Hee, J., Fortner, E., Shilling, J. E., Worsnop, D., Yokelson, R. J., Parworth, C., Ge, X., Xu, J., Butterfield, Z., Chand, D., Dubey, M. K., Pekour, M. S., Springston, S., and Zhang, Q.: Regional Influence of Aerosol Emissions from Wildfires Driven by
630   Combustion Efficiency: Insights from the BBOP Campaign, Environ. Sci. Technol., 50, 8613–8622, https://doi.org/10.1021/acs.est.6b01617, 2016.

Costabile, F., Barnaba, F., Angelini, F., and Gobbi, G. P.: Identification of key aerosol populations through their size and composition resolved spectral scattering and absorption, Atmos. Chem. Phys., 13, 2455–2470, https://doi.org/10.5194/acp-13-2455-2013, 2013.

635   Cubison, M. J., Ortega, A. M., Hayes, P. L., Farmer, D. K., Day, D., Lechner, M. J., Brune, W. H., Apel, E., Diskin, G. S., Fisher, J. A., Fuelberg, H. E., Hecobian, A., Knapp, D. J., Mikoviny, T., Riemer, D., Sachse, G. W., Sessions, W., Weber, R. J., Weinheimer, A. J., Wisthaler, A., and Jimenez, J. L.: Effects of aging on organic aerosol from open biomass burning smoke in aircraft and laboratory studies, Atmos. Chem. Phys., 11, 12049–12064, https://doi.org/10.5194/acp-11-12049-2011, 2011.

640   DeCarlo, P. F., Kimmel, J. R., Trimborn, A., Northway, M. J., Jayne, J. T., Aiken, A. C., Gonin, M., Fuhrer, K., Horvath, T., Docherty, K. S., Worsnop, D. R., and Jimenez, J. L.: Field-Deployable, High-Resolution, Time-of-

Flight Aerosol Mass Spectrometer, Anal. Chem., 78, 8281–8289, https://doi.org/10.1021/ac061249n, 2006.

Deng, X., Tie, X., Zhou, X., Wu, D., Zhong, L., Tan, H., Li, F., Huang, X., Bi, X., and Deng, T.: Effects of Southeast Asia biomass burning on aerosols and ozone concentrations over the Pearl River Delta (PRD) region, Atmos. Environ., 42, 8493–8501, https://doi.org/10.1016/j.atmosenv.2008.08.013, 2008.

Docherty, K. S., Stone, E. A., Ulbrich, I. M., DeCarlo, P. F., Snyder, D. C., Schauer, J. J., Peltier, R. E., Weber, R. J., Murphy, S. M., Seinfeld, J. H., Grover, B. D., Eatough, D. J., and Jimenez, J. L.: Apportionment of Primary and Secondary Organic Aerosols in Southern California during the 2005 Study of Organic Aerosols in Riverside (SOAR-1), Environ. Sci. Technol., 42, 7655–7662, https://doi.org/10.1021/es8008166, 2008.

Draxler, R. R. and Hess, G. D.: An overview of the HYSPLIT_4 modeling system for trajectories, dispersion, and deposition, Aust. Meteorol. Mag., 295–308, 1998.

Eck, T. F., Holben, B. N., Ward, D. E., Dubovik, O., Reid, J. S., Smirnov, A., Mukelabai, M. M., Hsu, N. C., O'Neill, N. T., and Slutsker, I.: Characterization of the optical properties of biomass burning aerosols in Zambia during the 1997 ZIBBEE field campaign, J. Geophys. Res. Atmos., 106, 3425–3448, https://doi.org/10.1029/2000JD900555, 2001.

Farmer, D. K., Matsunaga, A., Docherty, K. S., Surratt, J. D., Seinfeld, J. H., Ziemann, P. J., and Jimenez, J. L.: Response of an aerosol mass spectrometer to organonitrates and organosulfates and implications for atmospheric chemistry, Proc. Natl. Acad. Sci., 107, 6670–6675, https://doi.org/10.1073/pnas.0912340107, 2010.

Ferek, R. J., Reid, J. S., Hobbs, P. V., Blake, D. R., and Liousse, C.: Emission factors of hydrocarbons, halocarbons, trace gases and particles from biomass burning in Brazil, J. Geophys. Res. Atmos., 103, 32107–32118, https://doi.org/10.1029/98JD00692, 1998.

Fischer, E. V., Zhu, L., Payne, V. H., Worden, J. R., Jiang, Z., Kulawik, S. S., Brey, S., Hecobian, A., Gombos, D., Cady-Pereira, K., and Flocke, F.: Using TES retrievals to investigate PAN in North American biomass burning plumes, Atmos. Chem. Phys., 18, 5639–5653, https://doi.org/10.5194/acp-18-5639-2018, 2018.

Forrister, H., Liu, J., Scheuer, E., Dibb, J., Ziemba, L., Thornhill, K. L., Anderson, B., Diskin, G., Perring, A. E., Schwarz, J. P., Campuzano-Jost, P., Day, D. A., Palm, B. B., Jimenez, J. L., Nenes, A., and Weber, R. J.: Evolution of brown carbon in wildfire plumes, Geophys. Res. Lett., 42, 4623–4630, https://doi.org/10.1002/2015GL063897, 2015.

Forster, C., Wandinger, U., Wotawa, G., James, P., Mattis, I., Althausen, D., Simmonds, P., O'Doherty, S., Jennings, S. G., Kleefeld, C., Schneider, J., Trickl, T., Kreipl, S., Jäger, H., and Stohl, A.: Transport of boreal forest fire emissions from Canada to Europe, J. Geophys. Res. Atmos., 106, 22887–22906, https://doi.org/10.1029/2001JD900115, 2001.

Fraser, M. P. and Lakshmanan, K.: Using Levoglucosan as a Molecular Marker for the Long-Range Transport of Biomass Combustion Aerosols, Environ. Sci. Technol., 34, 4560–4564, https://doi.org/10.1021/es991229l, 2000.

de Gouw, J. A. and Warneke, C.: Measurements of volatile organic compounds in the earth's atmosphere using proton-transfer-reaction mass spectrometry, Mass Spectrom. Rev., 26, 223–257, https://doi.org/10.1002/mas.20119, 2007.

de Gouw, J. A., Warneke, C., Parrish, D. D., Holloway, J. S., Trainer, M., and Fehsenfeld, F. C.: Emission sources

and ocean uptake of acetonitrile (CH3CN) in the atmosphere, J. Geophys. Res. Atmos., 108, 1–8,

680   https://doi.org/10.1029/2002jd002897, 2003a.

de Gouw, J. A., Warneke, C., Karl, T., Eerdekens, G., van der Veen, C., and Fall, R.: Sensitivity and specificity of atmospheric trace gas detection by proton-transfer-reaction mass spectrometry, Int. J. Mass Spectrom., 223–224, 365–382, https://doi.org/10.1016/S1387-3806(02)00926-0, 2003b.

de Gouw, J. and Jimenez, J. L.: Organic Aerosols in the Earth's Atmosphere, Environ. Sci. Technol., 43, 7614–

685   7618, https://doi.org/10.1021/es9006004, 2009.

Grieshop, A. P., Donahue, N. M., and Robinson, A. L.: Laboratory investigation of photochemical oxidation of organic aerosol from wood fires 2: analysis of aerosol mass spectrometer data, Atmos. Chem. Phys., 9, 2227–2240, https://doi.org/10.5194/acp-9-2227-2009, 2009.

Guan, H., Wang, X., Han, R., Yuan, L., Meng, S., Wang, S., and Du, Z.: High-resolution and -precision spectra of

690   acetonitrile at the v5-band for laser remote sensing, J. Quant. Spectrosc. Radiat. Transf., 255, 107254, https://doi.org/10.1016/j.jqsrt.2020.107254, 2020.

Guo, F., Bui, A. A. T., Schulze, B. C., Yoon, S., Shrestha, S., Wallace, H. W., Sakai, Y., Actkinson, B. W., Erickson, M. H., Alvarez, S., Sheesley, R., Usenko, S., Flynn, J., and Griffin, R. J.: Urban core-downwind differences and relationships related to ozone production in a major urban area in Texas, Atmos. Environ., 262,

695   118624, https://doi.org/10.1016/j.atmosenv.2021.118624, 2021.

Gyawali, M., Arnott, W. P., Lewis, K., and Moosmüller, H.: In situ aerosol optics in Reno, NV, USA during and after the summer 2008 California wildfires and the influence of absorbing and non-absorbing organic coatings on spectral light absorption, Atmos. Chem. Phys., 9, 8007–8015, https://doi.org/10.5194/acp-9-8007-2009, 2009.

Hennigan, C. J., Miracolo, M. A., Engelhart, G. J., May, A. A., Presto, A. A., Lee, T., Sullivan, A. P., McMeeking,

700   G. R., Coe, H., Wold, C. E., Hao, W.-M., Gilman, J. B., Kuster, W. C., de Gouw, J., Schichtel, B. A., Collett, J. L., Kreidenweis, S. M., and Robinson, A. L.: Chemical and physical transformations of organic aerosol from the photo-oxidation of open biomass burning emissions in an environmental chamber, Atmos. Chem. Phys., 11, 7669–7686, https://doi.org/10.5194/acp-11-7669-2011, 2011.

Hobbs, P. V., Sinha, P., Yokelson, R. J., Christian, T. J., Blake, D. R., Gao, S., Kirchstetter, T. W., Novakov, T., and

705   Pilewskie, P.: Evolution of gases and particles from a savanna fire in South Africa, J. Geophys. Res. Atmos., 108, https://doi.org/10.1029/2002JD002352, 2003.

Holzinger, R., Warneke, C., Hansel, A., Jordan, A., Lindinger, W., Scharffe, D. H., Schade, G., and Crutzen, P. J.: Biomass burning as a source of formaldehyde, acetaldehyde, methanol, acetone, acetonitrile, and hydrogen cyanide, Geophys. Res. Lett., 26, 1161–1164, https://doi.org/10.1029/1999GL900156, 1999.

710   Holzinger, R., Jordan, A., Hansel, A., and Lindinger, W.: Automobile Emissions of Acetonitrile: Assessment of its Contribution to the Global Source, J. Atmos. Chem., 38(2), 187–193, https://doi.org/https://doi.org/10.1023/A:1006435723375, 2001.

Hu, W., Hu, M., Hu, W.-W., Niu, H., Zheng, J., Wu, Y., Chen, W., Chen, C., Li, L., Shao, M., Xie, S., and Zhang, Y.: Characterization of submicron aerosols influenced by biomass burning at a site in the Sichuan Basin,

715   southwestern China, Atmos. Chem. Phys., 16, 13213–13230, https://doi.org/10.5194/acp-16-13213-2016, 2016.

Huangfu, Y., Yuan, B., Wang, S., Wu, C., He, X., Qi, J., de Gouw, J., Warneke, C., Gilman, J. B., Wisthaler, A., Karl, T., Graus, M., Jobson, B. T., and Shao, M.: Revisiting Acetonitrile as Tracer of Biomass Burning in Anthropogenic-Influenced Environments, Geophys. Res. Lett., 48, https://doi.org/10.1029/2020GL092322, 2021.

Hung, W.-T., Lu, C.-H. (Sarah), Shrestha, B., Lin, H.-C., Lin, C.-A., Grogan, D., Hong, J., Ahmadov, R., James, E., and Joseph, E.: The impacts of transported wildfire smoke aerosols on surface air quality in New York State: A case study in summer 2018, Atmos. Environ., 227, 117415, https://doi.org/10.1016/j.atmosenv.2020.117415, 2020.

Inomata, S., Tanimoto, H., Fujitani, Y., Sekimoto, K., Sato, K., Fushimi, A., Yamada, H., Hori, S., Kumazawa, Y., Shimono, A., and Hikida, T.: On-line measurements of gaseous nitro-organic compounds in diesel vehicle exhaust by proton-transfer-reaction mass spectrometry, Atmos. Environ., 73, 195–203, https://doi.org/10.1016/j.atmosenv.2013.03.035, 2013.

Jaffe, D., Chand, D., Hafner, W., Westerling, A., and Spracklen, D.: Influence of Fires on O 3 Concentrations in the Western U.S., Environ. Sci. Technol., 42, 5885–5891, https://doi.org/10.1021/es800084k, 2008.

Jaffe, D. A., O'Neill, S. M., Larkin, N. K., Holder, A. L., Peterson, D. L., Halofsky, J. E., and Rappold, A. G.: Wildfire and prescribed burning impacts on air quality in the United States, J. Air Waste Manage. Assoc., 70, 583–615, https://doi.org/10.1080/10962247.2020.1749731, 2020.

Jefferson, A.: Empirical estimates of CCN from aerosol optical properties at four remote sites, Atmos. Chem. Phys., 10, 6855–6861, https://doi.org/10.5194/acp-10-6855-2010, 2010.

Jimenez, J. L., Canagaratna, M. R., Donahue, N. M., Prevot, A. S. H., Zhang, Q., Kroll, J. H., DeCarlo, P. F., Allan, J. D., Coe, H., Ng, N. L., Aiken, A. C., Docherty, K. S., Ulbrich, I. M., Grieshop, A. P., Robinson, A. L., Duplissy, J., Smith, J. D., Wilson, K. R., Lanz, V. A., Hueglin, C., Sun, Y. L., Tian, J., Laaksonen, A., Raatikainen, T., Rautiainen, J., Vaattovaara, P., Ehn, M., Kulmala, M., Tomlinson, J. M., Collins, D. R., Cubison, M. J., Dunlea, J., Huffman, J. A., Onasch, T. B., Alfarra, M. R., Williams, P. I., Bower, K., Kondo, Y., Schneider, J., Drewnick, F., Borrmann, S., Weimer, S., Demerjian, K., Salcedo, D., Cottrell, L., Griffin, R., Takami, A., Miyoshi, T., Hatakeyama, S., Shimono, A., Sun, J. Y., Zhang, Y. M., Dzepina, K., Kimmel, J. R., Sueper, D., Jayne, J. T., Herndon, S. C., Trimborn, A. M., Williams, L. R., Wood, E. C., Middlebrook, A. M., Kolb, C. E., Baltensperger, U., and Worsnop, D. R.: Evolution of Organic Aerosols in the Atmosphere, Science (80-.)., 326, 1525–1529, https://doi.org/10.1126/science.1180353, 2009.

Jobson, B. T. and McCoskey, J. K.: Sample drying to improve HCHO measurements by PTR-MS instruments: laboratory and field measurements, Atmos. Chem. Phys., 10, 1821–1835, https://doi.org/10.5194/acp-10-1821-2010, 2010.

Jobson, B. T., Volkamer, R. A., Velasco, E., Allwine, G., Westberg, H., Lamb, B. K., Alexander, M. L., Berkowitz, C. M., and Molina, L. T.: Comparison of aromatic hydrocarbon measurements made by PTR-MS, DOAS and GC-FID during the MCMA 2003 Field Experiment, Atmos. Chem. Phys., 10, 1989–2005, https://doi.org/10.5194/acp-10-1989-2010, 2010.

Joo, T., Rivera-Rios, J. C., Takeuchi, M., Alvarado, M. J., and Ng, N. L.: Secondary Organic Aerosol Formation from Reaction of 3-Methylfuran with Nitrate Radicals, ACS Earth Sp. Chem., 3, 922–934, https://doi.org/10.1021/acsearthspacechem.9b00068, 2019.

Karl, T., Jobson, T., Kuster, W. C., Williams, E., Stutz, J., Shetter, R., Hall, S. R., Goldan, P., Fehsenfeld, F., and Lindinger, W.: Use of proton-transfer-reaction mass spectrometry to characterize volatile organic compound sources

755   at the La Porte super site during the Texas Air Quality Study 2000, J. Geophys. Res. Atmos., 108, 1–15, https://doi.org/10.1029/2002jd003333, 2003.

Kasischke, E. S. and Turetsky, M. R.: Recent changes in the fire regime across the North American boreal region—Spatial and temporal patterns of burning across Canada and Alaska, Geophys. Res. Lett., 33, L09703, https://doi.org/10.1029/2006GL025677, 2006.

760   Kirchstetter, T. W., Novakov, T., and Hobbs, P. V.: Evidence that the spectral dependence of light absorption by aerosols is affected by organic carbon, J. Geophys. Res. D Atmos., 109, 1–12, https://doi.org/10.1029/2004JD004999, 2004.

Kondo, Y., Matsui, H., Moteki, N., Sahu, L., Takegawa, N., Kajino, M., Zhao, Y., Cubison, M. J., Jimenez, J. L., Vay, S., Diskin, G. S., Anderson, B., Wisthaler, A., Mikoviny, T., Fuelberg, H. E., Blake, D. R., Huey, G.,

765   Weinheimer, A. J., Knapp, D. J., and Brune, W. H.: Emissions of black carbon, organic, and inorganic aerosols from biomass burning in North America and Asia in 2008, J. Geophys. Res., 116, D08204, https://doi.org/10.1029/2010JD015152, 2011.

Laing, J. R., Jaffe, D. A., and Hee, J. R.: Physical and optical properties of aged biomass burning aerosol from wildfires in Siberia and the Western USA at the Mt. Bachelor Observatory, Atmos. Chem. Phys., 16, 15185–15197,

770   https://doi.org/10.5194/acp-16-15185-2016, 2016.

Laing, J. R., Jaffe, D. A., and Sedlacek, III, A. J.: Comparison of Filter-based Absorption Measurements of Biomass Burning Aerosol and Background Aerosol at the Mt. Bachelor Observatory, Aerosol Air Qual. Res., 20, 663–678, https://doi.org/10.4209/aaqr.2019.06.0298, 2020.

Langford, A. O., Senff, C. J., Alvarez, R. J., Brioude, J., Cooper, O. R., Holloway, J. S., Lin, M. Y., Marchbanks, R.

775   D., Pierce, R. B., Sandberg, S. P., Weickmann, A. M., and Williams, E. J.: An overview of the 2013 Las Vegas Ozone Study (LVOS): Impact of stratospheric intrusions and long-range transport on surface air quality, Atmos. Environ., 109, 305–322, https://doi.org/10.1016/j.atmosenv.2014.08.040, 2015.

Lei, R., Talbot, R., Wang, Y., Wang, S.-C., and Estes, M.: Influence of Cold Fronts on Variability of Daily Surface O_3 over the Houston-Galveston-Brazoria Area in Texas USA during 2003–2016, Atmosphere (Basel)., 9, 159,

780   https://doi.org/10.3390/atmos9050159, 2018.

Levy, R. C., Remer, L. A., Mattoo, S., Vermote, E. F., and Kaufman, Y. J.: Second-generation operational algorithm: Retrieval of aerosol properties over land from inversion of Moderate Resolution Imaging Spectroradiometer spectral reflectance, J. Geophys. Res. Atmos., 112, 2006JD007811, https://doi.org/10.1029/2006JD007811, 2007.

785   Li, F., Zhang, X., and Kondragunta, S.: Biomass Burning in Africa: An Investigation of Fire Radiative Power Missed by MODIS Using the 375 m VIIRS Active Fire Product, Remote Sens., 12, 1561, https://doi.org/10.3390/rs12101561, 2020.

Lindinger, W. and Jordan, A.: Proton-transfer-reaction mass spectrometry (PTR–MS): on-line monitoring of volatile organic compounds at pptv levels, Chem. Soc. Rev., 27, 347, https://doi.org/10.1039/a827347z, 1998.

790 Liu, X., Zhang, Y., Huey, L. G., Yokelson, R. J., Wang, Y., Jimenez, J. L., Campuzano-Jost, P., Beyersdorf, A. J., Blake, D. R., Choi, Y., St. Clair, J. M., Crounse, J. D., Day, D. A., Diskin, G. S., Fried, A., Hall, S. R., Hanisco, T. F., King, L. E., Meinardi, S., Mikoviny, T., Palm, B. B., Peischl, J., Perring, A. E., Pollack, I. B., Ryerson, T. B., Sachse, G., Schwarz, J. P., Simpson, I. J., Tanner, D. J., Thornhill, K. L., Ullmann, K., Weber, R. J., Wennberg, P. O., Wisthaler, A., Wolfe, G. M., and Ziemba, L. D.: Agricultural fires in the southeastern U.S. during SEAC 4 RS:

795 Emissions of trace gases and particles and evolution of ozone, reactive nitrogen, and organic aerosol, J. Geophys. Res. Atmos., 121, 7383–7414, https://doi.org/10.1002/2016JD025040, 2016.

Markowicz, K. M., Chilinski, M. T., Lisok, J., Zawadzka, O., Stachlewska, I. S., Janicka, L., Rozwadowska, A., Makuch, P., Pakszys, P., Zielinski, T., Petelski, T., Posyniak, M., Pietruczuk, A., Szkop, A., and Westphal, D. L.: Study of aerosol optical properties during long-range transport of biomass burning from Canada to Central Europe

800 in July 2013, J. Aerosol Sci., 101, 156–173, https://doi.org/10.1016/j.jaerosci.2016.08.006, 2016.

Marley, N. A., Gaffney, J. S., Tackett, M., Sturchio, N. C., Heraty, L., Martinez, N., Hardy, K. D., Marchany-Rivera, A., Guilderson, T., MacMillan, A., and Steelman, K.: The impact of biogenic carbon sources on aerosol absorption in Mexico City, Atmos. Chem. Phys., 9, 1537–1549, https://doi.org/10.5194/acp-9-1537-2009, 2009.

Mathur, R.: Estimating the impact of the 2004 Alaskan forest fires on episodic particulate matter pollution over the

805 eastern United States through assimilation of satellite-derived aerosol optical depths in a regional air quality model, J. Geophys. Res., 113, D17302, https://doi.org/10.1029/2007JD009767, 2008.

McMillan, W. W., Pierce, R. B., Sparling, L. C., Osterman, G., McCann, K., Fischer, M. L., Rappenglück, B., Newsom, R., Turner, D., Kittaka, C., Evans, K., Biraud, S., Lefer, B., Andrews, A., and Oltmans, S.: An observational and modeling strategy to investigate the impact of remote sources on local air quality: A Houston,

810 Texas, case study from the Second Texas Air Quality Study (TexAQS II), J. Geophys. Res., 115, D01301, https://doi.org/10.1029/2009JD011973, 2010.

Mehra, M., Panday, A. K., Puppala, S. P., Sapkota, V., Adhikary, B., Pokheral, C. P., and Ram, K.: Impact of local and regional emission sources on air quality in foothills of the Himalaya during spring 2016: An observation, satellite and modeling perspective, Atmos. Environ., 216, 116897, https://doi.org/10.1016/j.atmosenv.2019.116897,

815 2019.

Morris, G. A., Hersey, S., Thompson, A. M., Pawson, S., Nielsen, J. E., Colarco, P. R., McMillan, W. W., Stohl, A., Turquety, S., Warner, J., Johnson, B. J., Kucsera, T. L., Larko, D. E., Oltmans, S. J., and Witte, J. C.: Alaskan and Canadian forest fires exacerbate ozone pollution over Houston, Texas, on 19 and 20 July 2004, J. Geophys. Res., 111, D24S03, https://doi.org/10.1029/2006JD007090, 2006.

820 Ng, N. L., Canagaratna, M. R., Zhang, Q., Jimenez, J. L., Tian, J., Ulbrich, I. M., Kroll, J. H., Docherty, K. S., Chhabra, P. S., Bahreini, R., Murphy, S. M., Seinfeld, J. H., Hildebrandt, L., Donahue, N. M., DeCarlo, P. F., Lanz, V. A., Prévôt, A. S. H., Dinar, E., Rudich, Y., and Worsnop, D. R.: Organic aerosol components observed in Northern Hemispheric datasets from Aerosol Mass Spectrometry, Atmos. Chem. Phys., 10, 4625–4641, https://doi.org/10.5194/acp-10-4625-2010, 2010.

825 O'Neill, N. T., Eck, T. F., Holben, B. N., Smirnov, A., Royer, A., and Li, Z.: Optical properties of boreal forest fire smoke derived from Sun photometry, J. Geophys. Res. Atmos., 107, AAC 6-1-AAC 6-19,

https://doi.org/10.1029/2001JD000877, 2002.

Ogren, J. A., Wendell, J., Andrews, E., and Sheridan, P. J.: Continuous light absorption photometer for long-term studies, Atmos. Meas. Tech., 10, 4805–4818, https://doi.org/10.5194/amt-10-4805-2017, 2017.

830   Oltmans, S. J., Lefohn, A. S., Harris, J. M., and Shadwick, D. S.: Background ozone levels of air entering the west coast of the US and assessment of longer-term changes, Atmos. Environ., 42, 6020–6038, https://doi.org/10.1016/j.atmosenv.2008.03.034, 2008.

Paatero, P. and Tapper, U.: Positive matrix factorization: A non-negative factor model with optimal utilization of error estimates of data values, Environmetrics, 5, 111–126, https://doi.org/10.1002/env.3170050203, 1994.

835   Pandolfi, M., Alados-Arboledas, L., Alastuey, A., Andrade, M., Angelov, C., Artiñano, B., Backman, J., Baltensperger, U., Bonasoni, P., Bukowiecki, N., Collaud Coen, M., Conil, S., Coz, E., Crenn, V., Dudoitis, V., Ealo, M., Eleftheriadis, K., Favez, O., Fetfatzis, P., Fiebig, M., Flentje, H., Ginot, P., Gysel, M., Henzing, B., Hoffer, A., Holubova Smejkalova, A., Kalapov, I., Kalivitis, N., Kouvarakis, G., Kristensson, A., Kulmala, M., Lihavainen, H., Lunder, C., Luoma, K., Lyamani, H., Marinoni, A., Mihalopoulos, N., Moerman, M., Nicolas, J.,

840   O'Dowd, C., Petäjä, T., Petit, J.-E., Pichon, J. M., Prokopciuk, N., Putaud, J.-P., Rodríguez, S., Sciare, J., Sellegri, K., Swietlicki, E., Titos, G., Tuch, T., Tunved, P., Ulevicius, V., Vaishya, A., Vana, M., Virkkula, A., Vratolis, S., Weingartner, E., Wiedensohler, A., and Laj, P.: A European aerosol phenomenology – 6: scattering properties of atmospheric aerosol particles from 28 ACTRIS sites, Atmos. Chem. Phys., 18, 7877–7911, https://doi.org/10.5194/acp-18-7877-2018, 2018.

845   Parrish, D. D., Allen, D. T., Bates, T. S., Estes, M., Fehsenfeld, F. C., Feingold, G., Ferrare, R., Hardesty, R. M., Meagher, J. F., Nielsen-Gammon, J. W., Pierce, R. B., Ryerson, T. B., Seinfeld, J. H., and Williams, E. J.: Overview of the Second Texas Air Quality Study (TexAQS II) and the Gulf of Mexico Atmospheric Composition and Climate Study (GoMACCS), J. Geophys. Res., 114, D00F13, https://doi.org/10.1029/2009JD011842, 2009.

Pokhrel, R. P., Wagner, N. L., Langridge, J. M., Lack, D. A., Jayarathne, T., Stone, E. A., Stockwell, C. E.,

850   Yokelson, R. J., and Murphy, S. M.: Parameterization of single-scattering albedo (SSA) and absorption Ångström exponent (AAE) with EC/OC for aerosol emissions from biomass burning, Atmos. Chem. Phys., 16, 9549–9561, https://doi.org/10.5194/acp-16-9549-2016, 2016.

Ramanathan, V., Crutzen, P. J., Kiehl, J. T., and Rosenfeld, D.: Aerosols, Climate, and the Hydrological Cycle, Science (80-.)., 294, 2119–2124, https://doi.org/10.1126/science.1064034, 2001.

855   Reid, J. S., Eck, T. F., Christopher, S. A., Koppmann, R., Dubovik, O., Eleuterio, D. P., Holben, B. N., Reid, E. A., and Zhang, J.: A review of biomass burning emissions part III: intensive optical properties of biomass burning particles, Atmos. Chem. Phys., 5, 827–849, https://doi.org/10.5194/acp-5-827-2005, 2005.

Remer, L. A., Kaufman, Y. J., Tanré, D., Mattoo, S., Chu, D. A., Martins, J. V., Li, R.-R., Ichoku, C., Levy, R. C., Kleidman, R. G., Eck, T. F., Vermote, E., and Holben, B. N.: The MODIS Aerosol Algorithm, Products, and

860   Validation, J. Atmos. Sci., 62, 947–973, https://doi.org/10.1175/JAS3385.1, 2005.

Rogers, C. M. and Bowman, K. P.: Transport of smoke from the Central American fires of 1998, J. Geophys. Res. Atmos., 106, 28357–28368, https://doi.org/10.1029/2000JD000187, 2001.

Rogers, H. M., Ditto, J. C., and Gentner, D. R.: Evidence for impacts on surface-level air quality in the northeastern

US from long-distance transport of smoke from North American fires during the Long Island Sound Tropospheric

865   Ozone Study (LISTOS) 2018, Atmos. Chem. Phys., 20, 671–682, https://doi.org/10.5194/acp-20-671-2020, 2020.

Rolph, G. D., Draxler, R. R., Stein, A. F., Taylor, A., Ruminski, M. G., Kondragunta, S., Zeng, J., Huang, H.-C.,

Manikin, G., McQueen, J. T., and Davidson, P. M.: Description and Verification of the NOAA Smoke Forecasting

System: The 2007 Fire Season, Weather Forecast., 24, 361–378, https://doi.org/10.1175/2008WAF2222165.1, 2009.

Russell, P. B., Bergstrom, R. W., Shinozuka, Y., Clarke, A. D., Decarlo, P. F., Jimenez, J. L., and Livingston, J. M.:

870   Absorption Angstrom Exponent in AERONET and related data as an indicator of aerosol composition, Atmos.

Chem. Phys., 1155–1169, 2010.

Sakamoto, K. M., Allan, J. D., Coe, H., Taylor, J. W., Duck, T. J., and Pierce, J. R.: Aged boreal biomass-burning

aerosol size distributions from BORTAS 2011, Atmos. Chem. Phys., 15, 1633–1646, https://doi.org/10.5194/acp-

15-1633-2015, 2015.

875   Schade, G. W., Khan, S., Park, C., and Boedeker, I.: Rural Southeast Texas Air Quality Measurements during the

2006 Texas Air Quality Study, J. Air Waste Manage. Assoc., 61, 1070–1081,

https://doi.org/10.1080/10473289.2011.608621, 2011.

Schmeisser, L., Andrews, E., Ogren, J. A., Sheridan, P., Jefferson, A., Sharma, S., Kim, J. E., Sherman, J. P.,

Sorribas, M., Kalapov, I., Arsov, T., Angelov, C., Mayol-Bracero, O. L., Labuschagne, C., Kim, S.-W., Hoffer, A.,

880   Lin, N.-H., Chia, H.-P., Bergin, M., Sun, J., Liu, P., and Wu, H.: Classifying aerosol type using in situ surface

spectral aerosol optical properties, Atmos. Chem. Phys., 17, 12097–12120, https://doi.org/10.5194/acp-17-12097-

2017, 2017.

Schuster, G. L., Dubovik, O., and Holben, B. N.: Angstrom exponent and bimodal aerosol size distributions, J.

Geophys. Res. Atmos., 111, 1–14, https://doi.org/10.1029/2005JD006328, 2006.

885   Sciare, J., Oikonomou, K., Favez, O., Liakakou, E., Markaki, Z., Cachier, H., and Mihalopoulos, N.: Long-term

measurements of carbonaceous aerosols in the Eastern Mediterranean: evidence of long-range transport of biomass

burning, Atmos. Chem. Phys., 8, 5551–5563, https://doi.org/10.5194/acp-8-5551-2008, 2008.

Shrestha, S., Puppala, S. P., Adhikary, B., Shrestha, K. L., and Panday, A. K.: Field Measurements for Quantifying

Semi-Volatile Aerosol Influence on Physical and Optical Properties of Ambient Aerosols in the Kathmandu Valley,

890   Nepal, Aerosol Air Qual. Res., https://doi.org/10.4209/aaqr.2017.11.0492, 2018.

Shrestha, S., Yoon, S., Erickson, M. H., Guo, F., Mehra, M., Bui, A. A. T., Schulze, B. C., Kotsakis, A., Daube, C.,

Herndon, S. C., Yacovitch, T. I., Alvarez, S., Flynn, J. H., Griffin, R. J., Cobb, G. P., Usenko, S., and Sheesley, R.

J.: Traffic, transport, and vegetation drive VOC concentrations in a major urban area in Texas, Sci. Total Environ.,

155861, https://doi.org/10.1016/j.scitotenv.2022.155861, 2022.

895   Singh, H. B., Cai, C., Kaduwela, A., Weinheimer, A., and Wisthaler, A.: Interactions of fire emissions and urban

pollution over California: Ozone formation and air quality simulations, Atmos. Environ., 56, 45–51,

https://doi.org/10.1016/j.atmosenv.2012.03.046, 2012.

Sinha, V., Kumar, V., and Sarkar, C.: Chemical composition of pre-monsoon air in the Indo-Gangetic Plain

measured using a new air quality facility and PTR-MS: high surface ozone and strong influence of biomass burning,

900   Atmos. Chem. Phys., 14, 5921–5941, https://doi.org/10.5194/acp-14-5921-2014, 2014.

Stein, A. F., Draxler, R. R., Rolph, G. D., Stunder, B. J. B., Cohen, M. D., and Ngan, F.: NOAA's HYSPLIT Atmospheric Transport and Dispersion Modeling System, Bull. Am. Meteorol. Soc., 96, 2059–2077, https://doi.org/10.1175/BAMS-D-14-00110.1, 2015.

Streets, D. G., Yarber, K. F., Woo, J.-H., and Carmichael, G. R.: Biomass burning in Asia: Annual and seasonal
905   estimates and atmospheric emissions, Global Biogeochem. Cycles, 17, n/a-n/a, https://doi.org/10.1029/2003GB002040, 2003.

Swarthout, R. F., Russo, R. S., Zhou, Y., Hart, A. H., and Sive, B. C.: Volatile organic compound distributions during the NACHTT campaign at the Boulder Atmospheric Observatory: Influence of urban and natural gas sources, J. Geophys. Res. Atmos., 118, 10,614-10,637, https://doi.org/10.1002/jgrd.50722, 2013.

910   Takegawa, N., Miyakawa, T., Kawamura, K., and Kondo, Y.: Contribution of Selected Dicarboxylic and ω-Oxocarboxylic Acids in Ambient Aerosol to the m/z 44 Signal of an Aerodyne Aerosol Mass Spectrometer, Aerosol Sci. Technol., 41, 418–437, https://doi.org/10.1080/02786820701203215, 2007.

Thompson, A. M., Smit, H. G. J., Witte, J. C., Stauffer, R. M., Johnson, B. J., Morris, G., von der Gathen, P., Van Malderen, R., Davies, J., Piters, A., Allaart, M., Posny, F., Kivi, R., Cullis, P., Hoang Anh, N. T., Corrales, E.,
915   Machinini, T., da Silva, F. R., Paiman, G., Thiong'o, K., Zainal, Z., Brothers, G. B., Wolff, K. R., Nakano, T., Stübi, R., Romanens, G., Coetzee, G. J. R., Diaz, J. A., Mitro, S., Mohamad, M., and Ogino, S.-Y.: Ozonesonde Quality Assurance: The JOSIE–SHADOZ (2017) Experience, Bull. Am. Meteorol. Soc., 100, 155–171, https://doi.org/10.1175/BAMS-D-17-0311.1, 2019.

Tiitta, P., Leskinen, A., Hao, L., Yli-Pirilä, P., Kortelainen, M., Grigonyte, J., Tissari, J., Lamberg, H., Hartikainen,
920   A., Kuuspalo, K., Kortelainen, A.-M., Virtanen, A., Lehtinen, K. E. J., Komppula, M., Pieber, S., Prévôt, A. S. H., Onasch, T. B., Worsnop, D. R., Czech, H., Zimmermann, R., Jokiniemi, J., and Sippula, O.: Transformation of logwood combustion emissions in a smog chamber: formation of secondary organic aerosol and changes in the primary organic aerosol upon daytime and nighttime aging, Atmos. Chem. Phys., 16, 13251–13269, https://doi.org/10.5194/acp-16-13251-2016, 2016.

925   Titos, G., Jefferson, A., Sheridan, P. J., Andrews, E., Lyamani, H., Alados-Arboledas, L., and Ogren, J. A.: Aerosol light-scattering enhancement due to water uptake during the TCAP campaign, Atmos. Chem. Phys., 14, 7031–7043, https://doi.org/10.5194/acp-14-7031-2014, 2014.

Tripathi, N., Sahu, L. K., Wang, L., Vats, P., Soni, M., Kumar, P., Satish, R. V., Bhattu, D., Sahu, R., Patel, K., Rai, P., Kumar, V., Rastogi, N., Ojha, N., Tiwari, S., Ganguly, D., Slowik, J., Prévôt, A. S. H., and Tripathi, S. N.:
930   Characteristics of VOC Composition at Urban and Suburban Sites of New Delhi, India in Winter, J. Geophys. Res. Atmos., 127, https://doi.org/10.1029/2021JD035342, 2022.

Tu, P., Hall, W. A., and Johnston, M. V.: Characterization of Highly Oxidized Molecules in Fresh and Aged Biogenic Secondary Organic Aerosol, Anal. Chem., 88, 4495–4501, https://doi.org/10.1021/acs.analchem.6b00378, 2016.

935   Valach, A. C., Langford, B., Nemitz, E., MacKenzie, A. R., and Hewitt, C. N.: Concentrations of selected volatile organic compounds at kerbside and background sites in central London, Atmos. Environ., 95, 456–467, https://doi.org/10.1016/j.atmosenv.2014.06.052, 2014.

Wang, S.-C., Wang, Y., Estes, M., Lei, R., Talbot, R., Zhu, L., and Hou, P.: Transport of Central American Fire Emissions to the U.S. Gulf Coast: Climatological pathways and impacts on ozone and PM 2.5, J. Geophys. Res. Atmos., https://doi.org/10.1029/2018JD028684, 2018.

Warneke, C., de Gouw, J. A., Stohl, A., Cooper, O. R., Goldan, P. D., Kuster, W. C., Holloway, J. S., Williams, E. J., Lerner, B. M., McKeen, S. A., Trainer, M., Fehsenfeld, F. C., Atlas, E. L., Donnelly, S. G., Stroud, V., Lueb, A., and Kato, S.: Biomass burning and anthropogenic sources of CO over New England in the summer 2004, J. Geophys. Res. Atmos., 111, https://doi.org/10.1029/2005JD006878, 2006.

Westerling, A. L. and Bryant, B. P.: Climate change and wildfire in California, Clim. Change, 87, 231–249, https://doi.org/10.1007/s10584-007-9363-z, 2008.

Westerling, A. L., Hidalgo, H. G., Cayan, D. R., and Swetnam, T. W.: Warming and Earlier Spring Increase Western U.S. Forest Wildfire Activity, Science (80-.)., 313, 940–943, https://doi.org/10.1126/science.1128834, 2006.

Wilkins, J. L., de Foy, B., Thompson, A. M., Peterson, D. A., Hyer, E. J., Graves, C., Fishman, J., and Morris, G. A.: Evaluation of Stratospheric Intrusions and Biomass Burning Plumes on the Vertical Distribution of Tropospheric Ozone Over the Midwestern United States, J. Geophys. Res. Atmos., 125, https://doi.org/10.1029/2020JD032454, 2020.

Wolfe, R. E., Lin, G., Nishihama, M., Tewari, K. P., Tilton, J. C., and Isaacman, A. R.: Suomi NPP VIIRS prelaunch and on-orbit geometric calibration and characterization, J. Geophys. Res. Atmos., 118, https://doi.org/10.1002/jgrd.50873, 2013.

Yokelson, R. J., Crounse, J. D., DeCarlo, P. F., Karl, T., Urbanski, S., Atlas, E., Campos, T., Shinozuka, Y., Kapustin, V., Clarke, A. D., Weinheimer, A., Knapp, D. J., Montzka, D. D., Holloway, J., Weibring, P., Flocke, F., Zheng, W., Toohey, D., Wennberg, P. O., Wiedinmyer, C., Mauldin, L., Fried, A., Richter, D., Walega, J., Jimenez, J. L., Adachi, K., Buseck, P. R., Hall, S. R., and Shetter, R.: Emissions from biomass burning in the Yucatan, Atmos. Chem. Phys., 9, 5785–5812, https://doi.org/10.5194/acp-9-5785-2009, 2009.

Yokelson, R. J., Andreae, M. O., and Akagi, S. K.: Pitfalls with the use of enhancement ratios or normalized excess mixing ratios measured in plumes to characterize pollution sources and aging, Atmos. Meas. Tech., 6, 2155–2158, https://doi.org/10.5194/amt-6-2155-2013, 2013.

Yoon, S., Ortiz, S. M., Clark, A. E., Barrett, T. E., Usenko, S., Duvall, R. M., Ruiz, L. H., Bean, J. K., Faxon, C. B., Flynn, J. H., Lefer, B. L., Leong, Y. J., Griffin, R. J., and Sheesley, R. J.: Apportioned primary and secondary organic aerosol during pollution events of DISCOVER-AQ Houston, Atmos. Environ., 244, 117954, https://doi.org/10.1016/j.atmosenv.2020.117954, 2021.

Zauscher, M. D., Wang, Y., Moore, M. J. K., Gaston, C. J., and Prather, K. A.: Air Quality Impact and Physicochemical Aging of Biomass Burning Aerosols during the 2007 San Diego Wildfires, Environ. Sci. Technol., 47, 7633–7643, https://doi.org/10.1021/es4004137, 2013.

Zhang, Q., Canagaratna, M. R., Jayne, J. T., Worsnop, D. R., and Jimenez, J. L.: Time- and size-resolved chemical composition of submicron particles in Pittsburgh: Implications for aerosol sources and processes, J. Geophys. Res., 110, D07S09, https://doi.org/10.1029/2004JD004649, 2005.

975   Zhang, Y.-N., Zhang, Z.-S., Chan, C.-Y., Engling, G., Sang, X.-F., Shi, S., and Wang, X.-M.: Levoglucosan and carbonaceous species in the background aerosol of coastal southeast China: case study on transport of biomass burning smoke from the Philippines, Environ. Sci. Pollut. Res., 19, 244–255, https://doi.org/10.1007/s11356-011-0548-7, 2012.

Zhou, S., Collier, S., Jaffe, D. A., Briggs, N. L., Hee, J., Sedlacek III, A. J., Kleinman, L., Onasch, T. B., and Zhang,
980   Q.: Regional influence of wildfires on aerosol chemistry in the western US and insights into atmospheric aging of biomass burning organic aerosol, Atmos. Chem. Phys., 17, 2477–2493, https://doi.org/10.5194/acp-17-2477-2017, 2017.

Zhou, S., Guo, F., Chao, C.-Y., Yoon, S., Alvarez, S. L., Shrestha, S., Flynn, J. H., Usenko, S., Sheesley, R. J., and Griffin, R. J.: Marine Submicron Aerosols from the Gulf of Mexico: Polluted and Acidic with Rapid Production of
985   Sulfate and Organosulfates, Environ. Sci. Technol., https://doi.org/10.1021/acs.est.2c05469, 2023.

Zhu, Q., Cao, L.-M., Tang, M.-X., Huang, X.-F., Saikawa, E., and He, L.-Y.: Characterization of Organic Aerosol at a Rural Site in the North China Plain Region: Sources, Volatility and Organonitrates, Adv. Atmos. Sci., 38, 1115–1127, https://doi.org/10.1007/s00376-020-0127-2, 2021.